Hochschule München University of Applied Sciences

Deutsches Zentrum für Luft- und Raumfahrt
German Aerospace Center

Bachelor Thesis:

# Stuck Actuator Fault Detection and Isolation on the MMX Rover


| | |
|---|---|
| Author: | Anna Merk |
| Course of Study: | Aerospace Engineering (LRB) |
| Matriculation Nr.: | 01486219 |
| Supervisor: | Prof. Dr.-Ing. Daniel Ossmann |
| Advisor at DLR: | Juliane Skibbe |
| Summer Semester: | 2023 |
| Submission Date: | 05. July 2023 |


Munich, July 2023

## Abstract

Since rovers for the exploration of celestial bodies are extremely expensive and long-term projects, it is crucial to avoid the collapse of these systems due to faults. Hence, the development of Fault Detection, Isolation, and Recovery (FDIR) systems for these rovers is indispensable. The MMX (Martian Moons Exploration) Rover is a small, wheeled rover created for the exploration of Mars moon Phobos as part of the MMX Mission by the Japanese Space Agency. In this thesis the problems of fault detection and fault isolation on one of the MMX Rover’s locomotion units are discussed. The objective is to answer the question of how to detect an immobilization fault in the rover's locomotion unit and how to differentiate on which constructional element the fault occurs.

To address this research topic, experiments are conducted to simulate the expected fault scenarios as well as normal operation. Specifically, the fault scenarios of a stuck wheel and a stuck leg are induced under various changing parameters, and torque and motor currents are measured. Additionally, baseline tests are performed to investigate the influence of Earth's gravity, motor drive velocity and direction of rotation. The values of nominal and faulty operations are compared in order to establish thresholds for fault detection. Machine learning techniques based on logistic regression are employed to enable fault isolation.

The results of the baseline tests show dependency of the torque and current measurements on all mentioned baseline test parameters. The evaluation using the methods described demonstrates reliable error detection through a torque threshold. Furthermore, the classification algorithm enables 95% accurate determination of the fault location.

# Kurzfassung

Da Rover für die Erforschung von Himmelskörpern äußerst teure und langfristige Projekte sind, ist es entscheidend, das Versagen dieser Systeme aufgrund von Fehlern zu vermeiden. Die Entwicklung von Fault Detection, Isolation and Recovery (FDIR) Systemen für diese Fahrzeuge ist daher unverzichtbar. Der MMX (Martian Moons Exploration) Rover ist ein kleiner Rover auf Rädern, der im Rahmen der MMX-Mission von der Japanischen Raumfahrtagentur für die Erforschung des Marsmondes Phobos entwickelt wurde.

In dieser Arbeit werden Fehler-Detektion und Fehler-Isolation an einer der Lokomotionseinheiten des MMX Rovers diskutiert. Das Ziel ist es, die Frage zu beantworten, wie ein Festfahren in der Lokomotionseinheit des Rovers detektiert und lokalisiert werden kann, an welchem Bauteil der Fehler auftritt.

Um dieses Thema anzugehen, werden Experimente durchgeführt, welche die erwarteten Fehlerfälle, sowie den normalen Betrieb simulieren. Insbesondere werden die Szenarien eines blockierten Rads und eines blockierten Beins unter verschiedenen Parametern herbeigeführt, und Drehmoment sowie Motorströme gemessen. Zusätzlich werden Baseline-Tests durchgeführt, um den Einfluss der Schwerkraft der Erde, der Motordrehzahl und der Rotationsrichtung zu untersuchen. Die Werte für den Normalbetrieb und den fehlerhaften Betrieb werden verglichen, um Schwellenwerte für die Fehlererkennung festzulegen. Maschinelles Lernen, basierend auf logistischer Regression, wird eingesetzt, um die Fehlerisolation zu ermöglichen.

Die Ergebnisse der Baseline-Tests zeigen eine Abhängigkeit der Drehmoment- und Strommessungen von allen genannten Parametern. Die Auswertung mit den beschriebenen Methoden zeigt eine zuverlässige Fehlererkennung durch einen Drehmoment-Schwellenwert. Darüber hinaus ermöglicht der Klassifikationsalgorithmus eine 95% genaue Bestimmung des fehlerhaften Bauteils.

# Contents

# List of Figures

## List of Tables

# Abbreviations

| | |
|---|---|
| ADC | Analogue-to-digital Converter |
| CNES | Centre National d’Etudes Spatiales (French Space Agency) |
| CCW | Counter-clockwise |
| CW | Clockwise |
| DLR | Deutsches Zentrum für Luft- und Raumfahrt (German Aerospace Center) |
| FDD | Fault Detection and Diagnosis |
| FDI | Fault Detection and Isolation |
| FDIR | Fault Detection, Isolation and Recovery |
| FN | False Negative |
| FP | False Positive |
| HDRM | Hold Down and Release Mechanism |
| JAXA | Japan Aerospace Exploration Agency |
| LSS | Locomotion Subsystem |
| MMX | Martian Moon Exploration |
| SD | Standard Deviation |
| TP | True Positive |

# 1 Introduction

The exploration of Mars has been a longstanding goal of many space agencies worldwide. Driven by the scientific curiosity to better understand the Red Planet's geology, climate, and potential for life, as well as by the prospect of paving the way for future human missions and colonization efforts, a lot of information has been gathered since the mid-1990s. But while the exploration of Mars and its surface has become increasingly more popular in the last years, not much is known about the Martian moons Phobos and Deimos. A relatively recent area of focus for space agencies is the origin and composition of these small, irregularly shaped bodies. Knowledge of this could provide insights into the early history and evolution of the Martian system and moreover the planetary formation in our larger solar system. Martian moons exploration, MMX, is the new sample return mission planned by the Japan Aerospace Exploration Agency (JAXA) targeting the two Martian moons with the scheduled launch in 2024 and return to the Earth in 2029 [1].

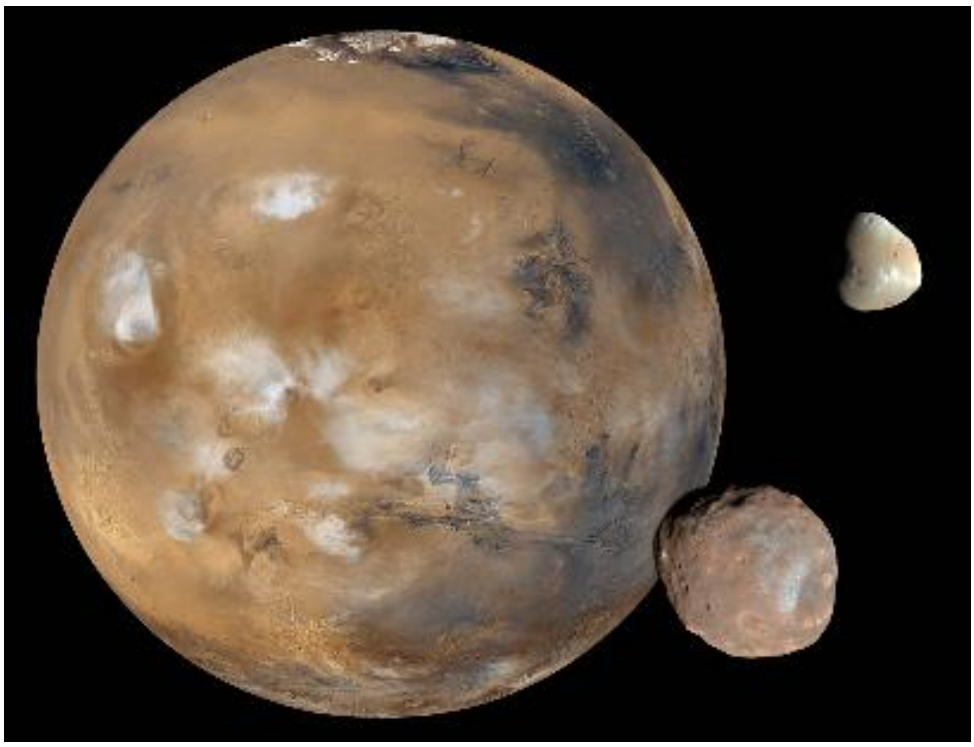

*Figure 1: Mars, Phobos and Deimos [2]*

As an additional component of the MMX mission, a small-sized rover (see Figure 2 and Figure 3) is being developed in collaboration with the German Aerospace Center (DLR) and the French space agency (CNES). This “MMX Rover” will be deployed on Phobos, the larger of the two moons of Mars, shown in Figure 1, where its goal is to conduct a more detailed investigation on the regolith properties. Phobos is almost 158 times smaller than the Moon, measuring only 22 kilometers in diameter and has a gravity of $0.0057\,\frac{\mathrm{m}}{\mathrm{s}^2}$, representing less than one

thousandth of Earth's gravity. On Phobos, a day lasts around seven Earth hours and temperatures range from -120° Celsius to +30° Celsius. The MMX Rover's mission will endure on this celestial body for 100 days.

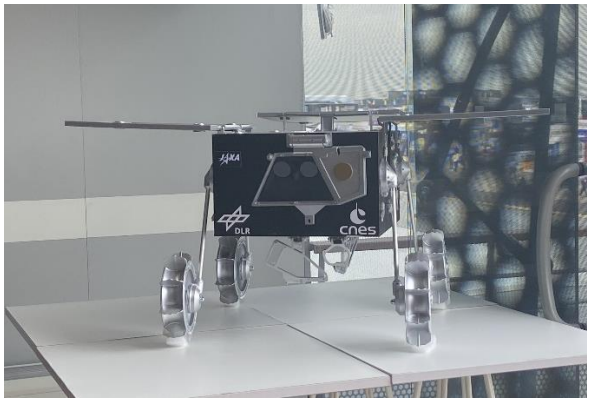


*Figure 2: MMX rover [3]*

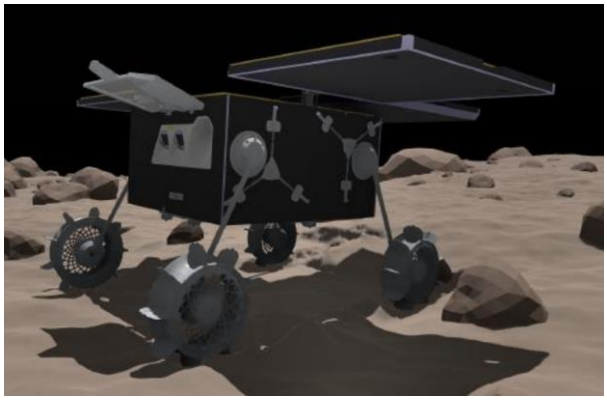

*Figure 3: MMX rover simulation in drive configuration [4]*

Even in highly sophisticated systems such as this rover, unforeseen faults can occur that threaten the success of the mission if they turn into a partial or complete failure of the system. An example of this worst case scenario is the Mars rover "Spirit", which got stuck in soft soil and whose mission was terminated after being unable to free itself [5].

It is therefore necessary to employ fault detection, isolation, and recovery procedures to be able to avoid this scenario. Within the scope of this thesis the possible faults of motor and actuator seizures due to external load induction will be addressed with a fault detection and isolation (FDI) methodology. The wheels as well as the legs could get stuck during operation, which, if undetected, can lead to damage or breakage of the mechanical parts or a depletion of power resources. An immediate shutdown of the locomotion system to stop all further movements is to be initiated in this scenario. After successful identification of the fault, appropriate recovery sequences can then be executed to resolve the issue. A series of experiments simulating the expected stuck fault conditions as closely as possible will therefore be conducted within the scope of this thesis. From these tests, threshold values shall be determined for certain sensors that show the presence of a fault in the system and thus will raise an alarm. Furthermore, a method shall be developed, that is able to derive from the measured sensor data if there is a fault and where the fault is located. The aim of this thesis is thus to propose an effective method to detect and isolate stuck faults on the MMX locomotion subsystem with the goal to provide enough knowledge on the rover's fault state to enable corrective actions for resolving the issue in the locomotion subsystem.

# 2 Theoretical Background - Fault Detection, Isolation and Recovery

Technical systems such as exploration rovers consist of a multitude of different sensors, actuators and mechanical as well as electrical components. A fault in a plant or its instrumentation can be defined as a deviation from the normal behavior caused by malfunctions of one or various elements of the system. An early detection of such faults is crucial for preventing performance degradation and machinery damage, which can in extreme cases lead to a loss of the system and thus, in the worst case, mission failure. Prompt and accurate diagnosis of a defective component through an analysis of a fault's characteristics enables optimal decision-making regarding corrective measures. The subfield of control engineering that concerns itself with the task of perceiving and identifying faults in a system, as well as providing reconfiguration methods with the goal to offer an optimal working technical system is commonly known as "Fault Detection, Isolation and Recovery", or in short FDIR.

According to Wander and Förstner [6], FDIR can be defined and implemented in many different ways. But the following three tasks present the main cornerstones of a modern FDIR system: Firstly, fault detection, in which the presence of a fault and its time of occurrence is determined. Next, isolation or identification respectively specify the type, location, and behavior of the fault, as well as its severity and possible effect on the system. Lastly the reconfiguration aims to compensate for the fault by, for instance, switching to redundant systems. In general, this approach is used to prevent faults from leading to catastrophic breakdowns of the plant, known as failures. The isolation and identification tasks together are referred to as fault diagnosis. Fault isolation follows the fault detection and describes the determination of the kind, location and time of detection of a fault. Fault identification by itself aims to determine supplementary information like the size and time-variant behavior of the fault. While detection is an absolute must in any practical system and isolation is almost equally important, fault identification may therefore not justify the extra effort it requires. Hence, most practical systems contain only the fault detection and isolation stages (and are referred to as FDI systems). [7], [8]

In control engineering faults are categorized in multiple ways, mainly by the effect they have and their temporal behavior. Multiplicative and additive faults are two types of errors, differentiated by their effect in systems. Multiplicative faults scale the values of affected variables, while additive faults introduce a constant shift to those values. Time behavior characteristics of faults are classified into abrupt faults that cause sudden, noticeable changes, incipient faults that develop gradually, and intermittent faults that occur sporadically.

In this thesis specifically, only fault detection and isolation are investigated. The following definitions apply to the technical terms mentioned before within this thesis.

- *Fault: A fault is the deviation of movement of the locomotion subsystem from its expected behavior, due to an actuator jamming on external parts.*

- *Detection: Fault Detection describes the process of identifying faulty behavior of the system through sensor measurements.*
- *Isolation: Fault Isolation is the task of differentiating between the different locations of the fault also through sensor data.*

Figure 4 shows the structural path of an exemplary fault detection and diagnosis (FDD) system from the fault to the fault diagnosis. First the fault impacts the process, from the measured signals the fault is detected, then the data known from the faulty measurements (symptoms) are handled by the fault isolation to classify the fault.

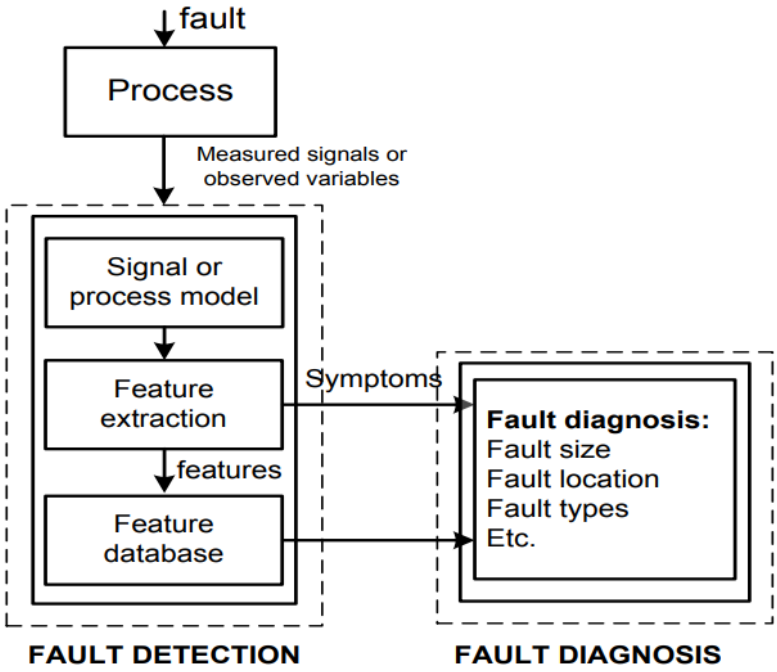


*Figure 4: Structure of FDI [9]*

## 2.1 Signal-, Model-, and Knowledge-based Fault Detection

There are several different methods to approach FDI, with the common goal being to raise an alarm when sensor data is detected that shows deviations from the nominal state. All methods consist of the same three basic cornerstones: the measurement data, a redundancy of information to these readings and a decision classifier. The difference between all approaches can be distinguished by the manner in which redundant information is provided. While signal-based fault detection works with the test readings alone, the knowledge-based technique relies on a great amount of historic data on which it was trained to recognize deviations. The analytical model-based fault detection requires a mathematical model of the system in question and

compares the expected outputs with the measurements to detect anomalies. The different procedures and their flow of data are shown in Figure 5. The top branch of the diagram presents the knowledge-based approach. The illustration shows that a significant amount of historic data is used for training and learning about the different faults to provide a solid knowledge base. Input data is then checked for consistency of fault patterns with the existing knowledge base. A classifier is then subsequently run through to decide if an alarm is triggered or not. In the middle of the figure the signal-based type of FDI is shown. Input data is processed by filtering or transformation to enable the enhanced observation of patterns and trends in the signal. Afterwards, the processed signal is checked for consistency with the known signal pattern before the result of that comparison is again passed through a classifier, that provides a decision on the triggering of an alarm as output. Lastly the diagram shows the model-based FDI method on the lowest branch. For this method the system in question first needs to be identified and a model needs to be developed that describes this system accurately. For this system its own classifier is set. During online operation the input data is then checked for consistency with the provided values from the mathematical model. The difference between these two values is called the residual. For this residual a threshold is set through a residual classifier which again provides the decision if a fault alarm is triggered or not.

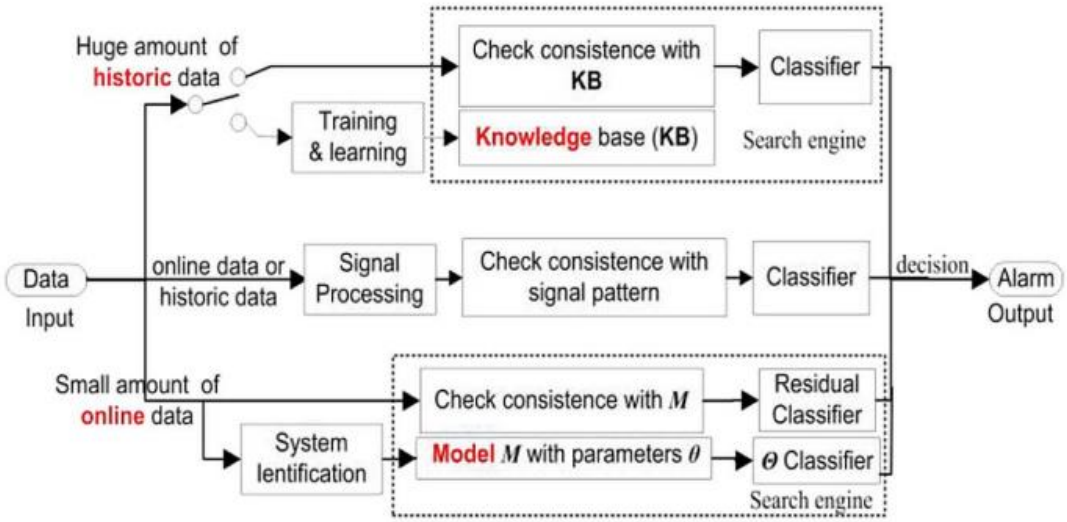


*Figure 5: Types of fault detection and isolation [10]*

Out of these three types of FDI, the method of highest simplicity is signal based, since it requires no knowledge of the mathematical workings of the system and no huge amount of training data. The signals can be processed through different filters or transformations to better observe certain patterns and tendencies. In the signal-based approach certain limit thresholds are then set for the plant measurements after processing. These can be upper and/or lower limits, as well as trend checks. If a reading exceeds a threshold, an alarm is raised. These so-called alarm systems are widely used in industrial applications, as no additional model or

knowledge of the plant is required. Significant shortcomings of this method, however, are the limited fault specificity and sensitivity. [11]

Next, there is the model-based approach. The fundamental idea of the model-based fault detection is an analytical redundancy, meaning the comparison of the plant outputs $y_i(t)$ with their analytically computed values $\hat{y}_i(t)$ obtained through the mathematical model. Both systems would receive the same command as input. The difference between the two values, the residual $e_i(t)$, is an indication of the possible presence of a system fault. [11], [12]

$$e_i(t) = y_i(t) - \hat{y}_i(t) \qquad (I)$$

As mentioned before, the model-based method requires an explicit mathematical model of the subsystem in question to be able to analytically investigate faults and develop suitable FDI algorithms. For systems where such a model is not available, due to a too high complexity or off-site intellectual properties that need to be protected, a last alternative approach can be taken: knowledge-based FDI. This method, also known as data-driven fault detection, relies on a great amount of historic data in nominal and faulty states of the system, that is then used for training and learning to detect faults and for fault isolation, recognize them by their patterns. According to Azam et al. [13], knowledge-driven schemes are chosen in scenarios, where all possible failure modes are known a priori and the system has a high number of sensors and therefore provides a high information density on the measurable state of the system. From the faults and the corresponding measured data, a decision matrix is created, depicting the characteristics of each single fault. This matrix can further be used to fuse different scenarios and therefore provide more sophisticated FDI solutions. A downside to this approach is the susceptibility to unknown faults, since only known fault scenarios are tested and therefore recognizable by the FDI system. Furthermore, large amounts of data are required to achieve satisfactory accuracy of the fault detection system.

## 2.2 Fault Isolation through Machine Learning

After successfully detecting a fault, the next crucial step involves determining the location and type of the fault - the so-called fault isolation. While detecting a fault usually requires simpler methods, such as setting up thresholds on certain measurements, fault isolation on the other hand generally necessitates more complex approaches, for instance machine learning.

Machine learning, a subfield of artificial intelligence, is dedicated to developing algorithms that can learn from data, recognize patterns, and make predictions or decisions without explicit programming instructions. These algorithms utilize statistical techniques to iteratively adjust their parameters and model representations based on observed data, enabling continuous improvement in their performance over time.

### 2.2.1 Characteristic Features

Once the fault is detected, the data measurements leading up to the fault threshold being exceeded are analyzed to isolate the specific fault responsible for the system's changed behavior. These measurements are checked for characteristic features, which are patterns in the data indicating different fault scenarios. Typical characteristic features include statistical information, such as the mean, average, standard deviation, minimum or maximum values recorded over specific timelines. Tests and system analyses help define the important characteristics of the measurement data for distinguishing faults. These "symptoms" are then stored in a database and compared with data from a new experiment. The goal is to predict the failure scenario by analyzing the symptoms and comparing them to previously known and labelled information about fault symptoms. This data-driven approach to isolating the different fault scenarios is also called knowledge-based isolation, since all conclusions drawn from the symptoms rely on the knowledge gathered beforehand. However, it is important to note that this technique can only identify "known" faults, which is one of its limitations.

### 2.2.2 Logistic Regression

In summary, applying the knowledge-based isolation method requires a significant number of recorded symptoms for known fault scenarios and one set of symptoms for the fault to be identified. The question remains, how an algorithm determines which fault is most likely to match the faulty measurements (symptoms). Data analysis that describes the relationship between a response (in this case the fault) and one or multiple predictor variables (in this case the symptoms) often relies on regression methods. Regression is a statistical method that explains or understands one variable based on one or more other variables. The variable that is being explained is called the dependent variable; the other variables used to explain or predict the response are called independent variables. Many times, independent variables are simply referred to as predictors. [14]

For problems where the dependent variable is not continuous, but instead falls into a finite number of discrete values, in the case of fault identification for example, this would mean predicting whether a certain fault is happening (1) or not (0). A simple linear regression is inadequate, as it assumes a linear relationship between the predictors and the response. In these cases, a logistic regression is used.

Logistic regression is a statistical algorithm that can be used for any classification problem where the target is a discrete (binary or ordinal) variable. Binary classification is aiming to predict one of two possible outcomes based on the input variables. It models the relationship between the input variables on the x-axis and the probability of the binary outcome on the y-axis using the logistic function (also known as the sigmoid function, see Figure 6).

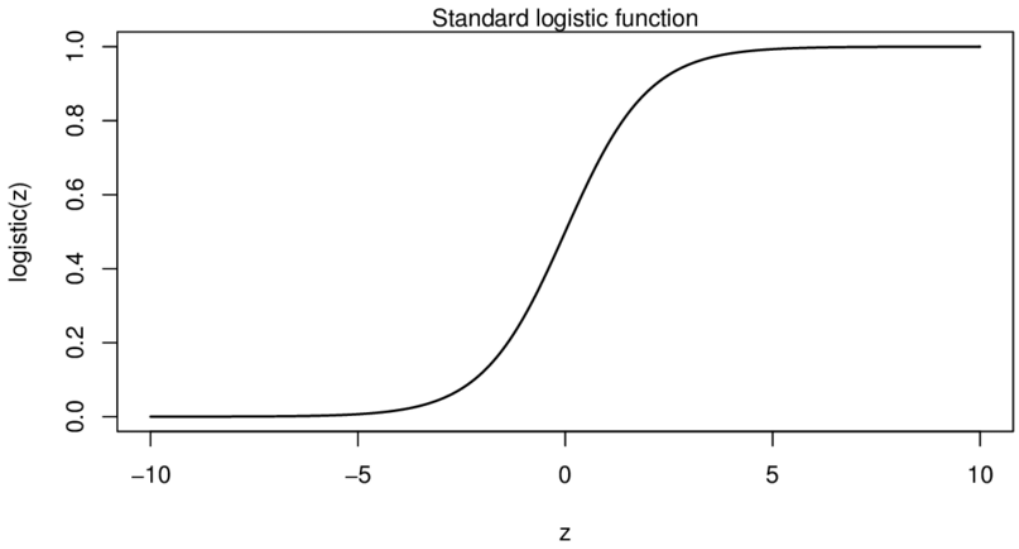


*Figure 6: Logistic function [15]*

Typically, if the probability of the scenario happening is over 50%, option 1 (fault is present) is considered to be true, while in the other cases, option 0 (fault is not present) is adopted. In comparison to other classification models, the logistic regression model permits the use of continuous and categorical predictors and provides the ability to adjust the model for multiple predictors at the same time. [16]

Logistic regression is a well-established statistical model widely used for binary classification problems. It assumes a linear relationship between independent variables and the log-odds of the dependent variable. When the relationships are indeed linear, logistic regression effectively captures and models the underlying associations between predictors and multiple classes. The linear assumption simplifies the model and allows for straightforward interpretation of the coefficients, facilitating an understanding of the impact of each independent variable on the probability of belonging to a specific class.

Logistic regression provides probabilistic predictions by estimating the probability of an observation belonging to each class based on the linear combination of independent variables. This feature is particularly advantageous in multiclass classification as it enables both classification and assessment of the uncertainty associated with predictions. By setting a decision threshold, observations can be assigned to the most probable class, taking into account the predicted probabilities.

On top of that logistic regression is computationally efficient and capable of handling large datasets with ease, making it a practical choice for multiclass classification problems involving linear relationships. Compared to more complex models, logistic regression does not require extensive computational resources and can be trained relatively quickly.

## 2.3 State of the Art FDI in Exploration Rovers

Research on the state of the art for fault detection and isolation in exploration rovers shows, that fault detection and isolation methods for this kind of plant can be based on a combination of continuous and discrete state estimation. Continuous state estimation on the one hand deals with systems or processes where the state variables can take on any value within a given range. Examples of continuous state estimation techniques include Kalman filtering, extended Kalman filtering, and particle filtering. These methods are commonly used in applications such as tracking systems, navigation systems, and control systems where the state variables change continuously over time. Discrete state estimation on the other hand deals with system where the state can only take on a finite set of distinct values. The change from one state to another is typically modelled as a step function. Discrete state estimation techniques involve probabilistic methods to infer the most likely state given the available information.[17]–[19]

Washington [17] presents an on-board method for continuous state estimation and fault diagnosis that uses Kalman filters and Markov-model representation in rovers. Dearden et al. [18] also describes particle filtering-based algorithms for state estimation that have been successfully demonstrated on diagnosis problems for rovers intended to be used on Martian missions. The literature research furthermore suggests that fault detection in planetary rovers specifically is a challenging problem due to the tight coupling between the rover's performance and its environment. Unlike spacecraft, rover performance depends significantly on environmental interactions. The on-board sensors provide streams of continuous valued data that varies due to noise, but also due to the interaction between the rover and its environment. A rover, for example, may have a sensor that reports the current drawn by a wheel. In normal operation this quantity may vary considerably, increasing when the vehicle is climbing a hill, and decreasing on downward slopes. The diagnosis system needs to be able to distinguish a change in the current drawn due to the terrain being traversed from a change due to a fault in the wheel. [20]

Traditional model-based diagnosis techniques are generally not suitable for these type of rovers due to the tight coupling between the vehicle’s performance and its environment, whereas hybrid diagnosis using particle or Kalman filters is presented as an alternative for continuous state estimation as described above [18], [20]. “Traditional approaches operate on discrete models and use monitors to translate continuous sensor readings into discrete values. The monitors are typically only used once the sensor readings have settled on a consistent value, and hence these systems cannot generally diagnose transient events. For many applications, e.g. planetary rovers, the complex dynamics of the system make reasoning with a discrete model inadequate.[…] To overcome this we need to reason directly with the continuous values we receive from sensors: Our model needs to be a hybrid system.” [18]

Kalman filters are optimal estimation algorithms. They solve the presented problem optimally for given weighting matrices that describe the stochastic properties of the signal. A Kalman filter can combine the information of all the sensors and give the optimal estimate of the actual position hence it is also known as a sensor fusion algorithm. Kalman filters are used when the state shall be estimated from various sensor measurements which are subject to noise. However, Kalman filters still require a mathematical model of the underlying process on top of the sensor measurements.

Following a different approach, Zanoli et al. [21] presents a data-driven, model-free technique based on Principal Components Analysis for fault detection and isolation in an unmanned surface vehicle.

The papers also discuss the importance of fault tolerance and the detection and diagnosis of faults in rovers [22]. Innovative fault detection techniques are proposed, and research challenges for the introduction of these methods in spacecraft FDIR systems are outlined [6]. The papers suggest that particle filtering-based algorithms for state estimation have been successfully demonstrated on diagnosis problems in planetary rovers, but there are challenges to make particle filters work in this domain, such as coping with high-dimensional continuous state spaces and severely constrained computational power [18].

In cases where no autonomous recovery is necessary, the isolation of the fault can be done on the ground instead of being implemented in the rover's system, avoiding the need for additional components, such as processors, on the rover to increase its computational power. In situations where enough computational power is available and solar panels provide enough power to run the fault identification onboard the rover, this is of course preferable. However, when this is not the case, and no autonomous recovery is necessary, stopping and waiting for a ground loop is the more obtainable solution. Here, only a fault detection method is strictly unavoidable on the rover itself, while everything else can be analyzed after the detection of such a fault to conclude and command the optimal recovery actions.

All of these approaches refer to technical systems that are similar in their requirements, environmental conditions and objectives to the FDI system of the MMX rover. However, they also differ in some key respects, which is why different methodologies are pursued in this work. Firstly, the fault cases to be detected are known and small in numbers. In the context of this work, only the specific fault cases of a stuck wheel and a stuck leg must be detected and distinguished from each other as well as from the normal state. In the context of this limitation and in view of the limited time resources for development, as well as the limitations of computational power and space on the rover itself, the use of simple approaches is favored. In addition, due to the lack of a mathematical model of the MMX rover and difficulties in creating such, the use of complex approaches such as particle and Kalman filtering is excluded.

# 3 The MMX Rover and the Locomotion Subsystem

The Locomotion Subsystem (LSS) of the MMX rover represents one of the most integral cornerstones for the success of its extra-terrestrial mission, as it is the primary system that enables movements and interaction with the surface of Phobos [23]. The LSS is responsible for the initial uprighting of the rover after landing, the self-positioning relative to the moon's surface, aligning the rover for sun-pointing, as well as driving and interacting with the ground. It is therefore essential that it is designed to be robust and fail-safe to ensure a successful exploration mission. The Locomotion system's mechanical design is guided by specific mission requirements. These objectives include surviving the impact of landing, supporting uprighting to allow unfolding of the solar panels, driving straight, making curves, and executing point turns to relocate the rover towards scientifically interesting locations on Phobos. Additionally, the system must be able to position and orient instruments and solar panels by adjusting the rover's position relative to the ground. All these functional requirements must be fulfilled while adhering to strict mass and volume limitations.

## 3.1 Mechanics of the Locomotion System

The rover's leg modules, shown in Figure 7, are comprised of two separate drivetrains, one for the shoulder and the other for the wheel rotation, respectively. In Figure 7, the shoulder module is highlighted. This is the location where all actuators and sensors are positioned on the inside of the rover chassis side panel. This placement serves to safeguard the electrical equipment from the extreme thermal conditions experienced during Phobos' seven earth-hour-long day, where temperatures range from -120° Celsius to +30° Celsius.

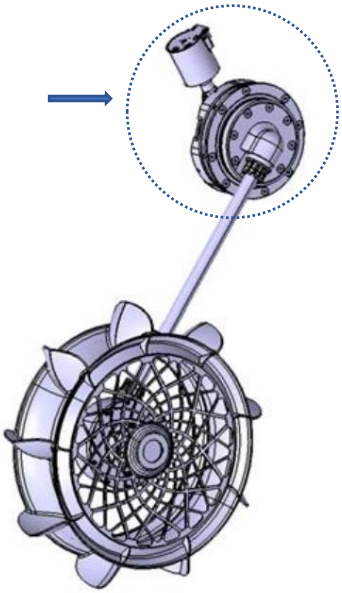

*Figure 7: One locomotion unit of the MMX rover [24]*

The wheel drivetrain is depicted in Figure 8. It mainly consists of a motor unit, which drives an internal running shaft through a bevel gear, which then in turn rotates the wheel through a crown gear. The overall ratio of translation from the motor-rotation to the wheel-rotation is 2227:1, providing “a uniform, yet extremely low traveling velocity […] while at the same time maintaining an adequate motor rotational speed” [25].

It should be noted that the bearings are unlubricated to avoid thermal issues, which in turn leads to increased friction during operation. This friction is also increased by the sealings on the wheel shaft, which intend to refrain small particles from the outside to cause damage to the mechanisms inside the wheel joint.

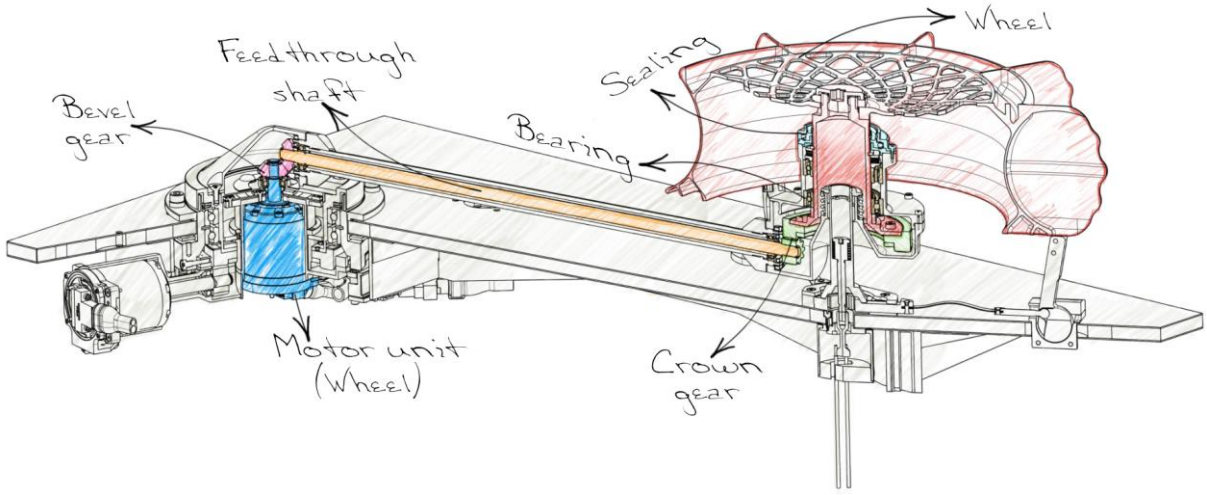


*Figure 8: Wheel drivetrain of the LSS [26]*

Figure 9 shows the similar mechanical setup of the shoulder drivetrain, which is built like a shell around the inner drivetrain for the wheel. A second motor unit with a pinion gear output shaft (shown in blue) directly drives the crown gear (depicted in green) which is attached to the output shaft (illustrated in red). The overall translation ratio of the shoulder drivetrain is the same as for the wheel, which is mentioned above. Included in the shoulder unit is also the torque sensor that measures the moments exerted onto the output shaft through external loads. To protect the inner workings of the shoulder drive mechanism from dust, debris, and harsh temperatures, sealings are put into place, which introduce friction to the system. Two different position sensors are installed in the shoulder joint, more information on these can be found in the next subchapter.

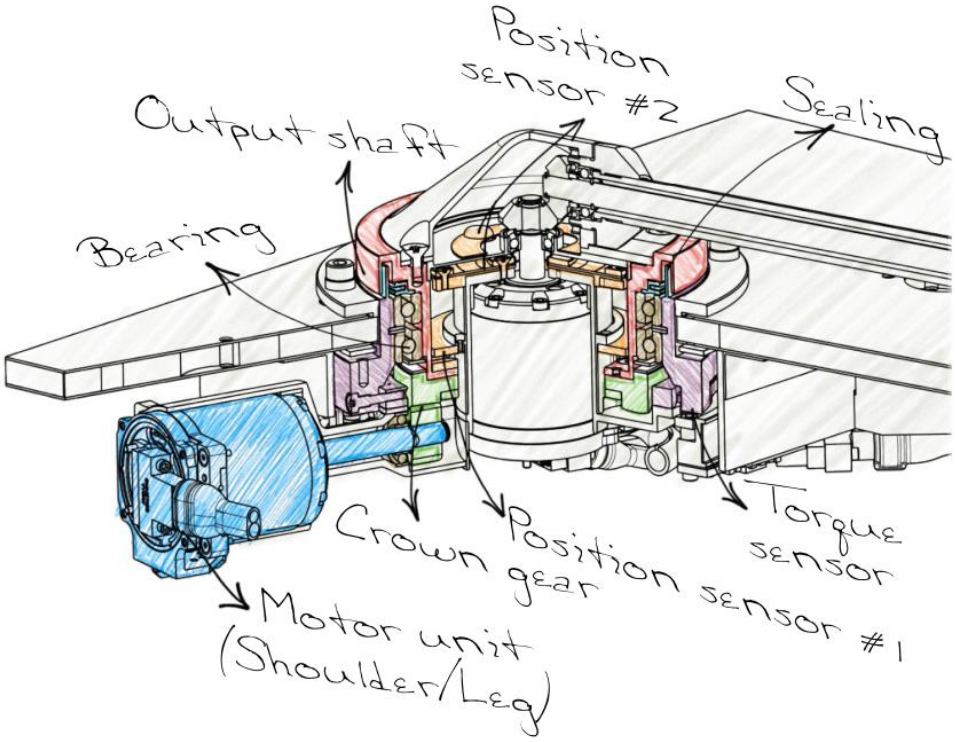


*Figure 9: Shoulder drivetrain of the LSS [26]*

One side panel of the rover with both legs mounted and locked in the hold-down and release mechanism HDRM is shown in Figure 10.

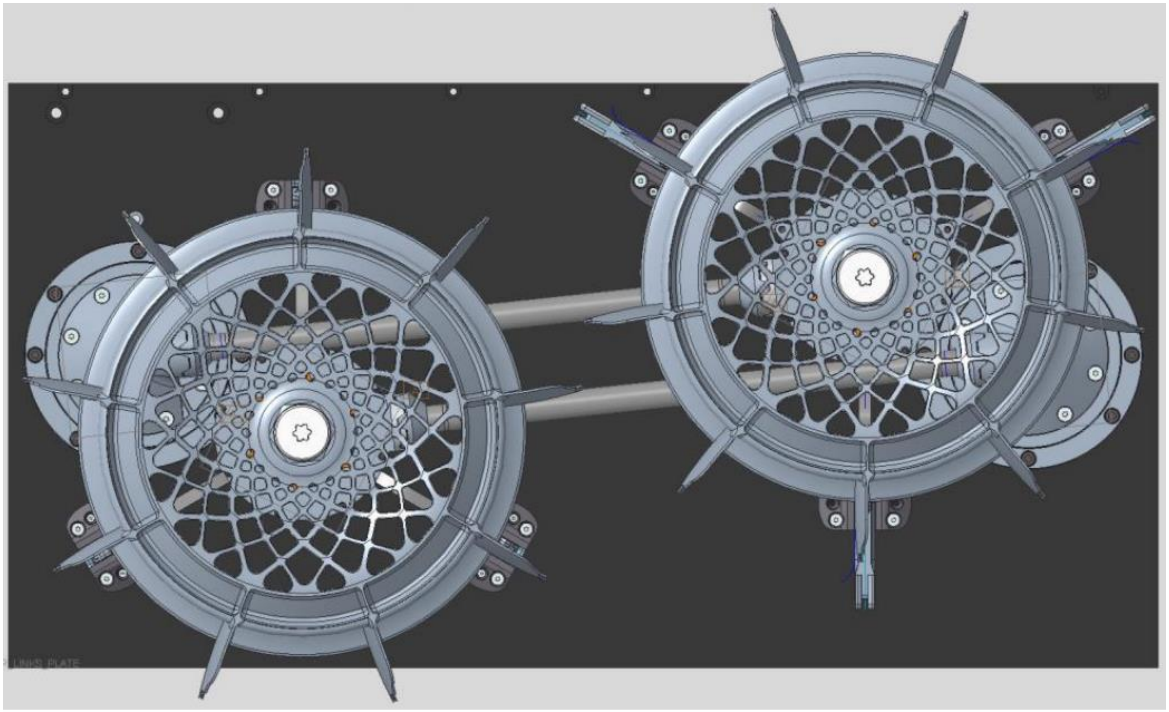

*Figure 10: Legs in stowed configuration*

## 3.2 Sensors

The Locomotion Subsystem of the MMX rover includes a variety of different sensors to monitor and trace its behavior. These sensors include [27]:

- one commutation sensor (Hall sensors) per motor
- one absolute position sensor (potentiometer) per leg
- one torque sensor per leg
- current sensors
- voltage sensors
- four 3-axis-accelerometers
- two single-axis-gyroscopes
- numerous temperature sensors
- a radiation sensor.

For the purpose of fault detection and isolation in this system not all of these sensors will be used, as some of their measurements would not provide more knowledge of the system's state for the specific fault cases of interest in this study. The focus of the fault analysis will be put on the motor position sensors (Hall Sensor and Potentiometer), as well as the torque and current sensors. As previously described in 3.1, all electronics, including all sensors, are located inside the shoulder module. Consequently, no absolute position sensor is installed for the wheel and all other measurements except for the shoulder torque, derive their data from the motors.
In summary, there are four measured values for the shoulder movement (current, relative position, absolute position, and torque) and two for the wheel movement (current and relative position). In the following passage the used sensors are described briefly.

### *Potentiometers*

For the measurement of the absolute position of the shoulder joint, a resistive potentiometer of a standard grabber type is installed on the output shaft of the shoulder drivetrain. For closer information on the used sensor see [28]. No absolute position of the wheel is measured.

### *Hall Sensors*

In each motor a commutation sensor is placed to measure the relative position change since the start of measurement. This serves as a redundant position sensor for the shoulder module and provides the possibility to track the wheel rotation and therefore also the travelled distance. The used hall effect sensors from Infineon [29] are positioned on the backside of the motor units.

### *Torque Sensor*

Since there is a comparably high friction in the Harmonic Drive gears, caused by the space lubrication, the possibility of a current measurement to obtain torque information is not possible. It is therefore necessary to implement a torque sensor into the shoulder module whose

main job is the detection of when the locomotion system gets stuck during operation, for instance between two boulders. The torque sensor is therefore one of the most important sensors in the task of isolating the faults within the LSS caused by external factors. The torque sensor integrated into the shoulder module of the locomotion unit is set to very low measurable moments due to the low-gravity environment on Phobos and the therefore very low expected torques during normal operation. The torque sensor has a measuring range of ±2 Newtonmeters. If this is exceeded the sensor will start to suffer plastic deformation and permanent destruction.

### *Motor Current Sensors*

On the Power Inverter and Control Board of the Locomotion System a single shunt current measurement for each power inverter is provided to supervise the motor currents and detect overcurrent conditions. The analogue signals of the motor current measurement are converted to digital form by the analogue-to-digital converters (ADCs) present on the board.

## 3.3 Fault Scenarios

As shown in the previous subchapters, the locomotion system is a complex mechanism that consists of various components that work together to provide movement. On top of the mechanical components described in the last chapters, a significant amount of software and controllers is involved in the execution of movements. Despite best design practices, faults can still occur in the LSS that can lead to malfunctions and even system failure. In general, there are four main fault types that can occur: sensor faults, software faults, mechanical faults and actuator faults. While each type of failure can have unique causes and consequences, for the purposes of this investigation, the focus lies specifically on the actuator faults that are caused by external loads or jamming. These pose a common risk of failure for locomotion systems on rovers that operate in remote environments, such as the Martian moon Phobos.
In this investigation two specific faults are of interest. Firstly, the rover's legs becoming stuck: If rocks or other debris is located between the leg of the rover and its side panel, a rotation of the shoulder joint could lead to the leg becoming stuck on the obstacle. Secondly the wheels of the MMX rover could become stuck on debris or lodged between boulders while traversing the Phobos surface. If a fault in these situations is not detected in time, structural damage to the motors, the sensors or the mechanical parts of the rover could be the outcome. It is therefore of very high importance to detect these fault situations through thresholds on the sensor measurements in real time and initiate a complete stop of movement before they lead to a permanent impact on the rover’s ability to maneuver and therefore potentially endanger the success of its scientific mission.

Given the long communication time between Earth and Phobos, as well as the limited availability of cameras to provide a complete assessment of the situation, it is also crucial that these faults are identifiable through the sensor data collected by the rover itself alone. With this in mind, the two different fault scenarios described - a stuck wheel and a stuck leg – are tested under various parameter changes, including different rotational speeds and directions on a test bench provided for this study, with the goal to establish functional fault detection and isolation methods for this specific system.

# 4 Fault Detection and Isolation Methodology

In this thesis the objective is to answer the question of how to detect an immobilization fault in the rover's locomotion unit and how to differentiate on which constructional element the fault occurs. This chapter explains the proposed FDI methodology to reach the goal of establishing a working fault detection and isolation system.

Through the FDI methodology two main problems shall be solved. Firstly, to detect a fault in the subsystem and secondly to isolate the fault in the subsystem. It is therefore split into the two sections seen in Figure 11: fault detection and fault isolation. For the detection of a fault onboard the MMX rover, thresholds shall be established on live sensor measurements, which, if exceeded, trigger a fault alarm, leading to a complete stop of all movement of the locomotion subsystem. After the triggering of such a fault, the recorded measurement data of the seconds preceding the exceedance of the threshold are fed through a classifier, which determines from the signal patterns which, if any, fault scenario is currently present. This FDI system provides the LSS with the possibility to enable effective corrective actions to revert the fault scenario and avoid damage to the system itself. The next two subchapters give an insight into how the two main cornerstones of this FDI system, the thresholds, and the classifier, are established.

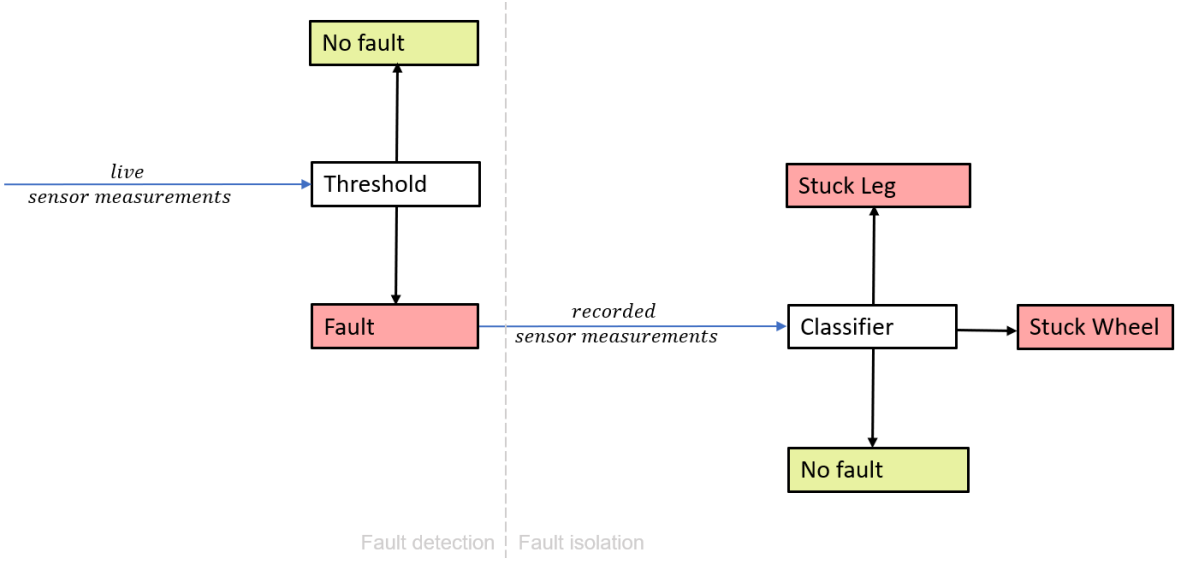


*Figure 11: FDI methodology*

## 4.1 Signal-based Approach for Fault Detection

For fault detection, a signal-based method relying solely on the measurements is chosen. To ensure reliable fault detection in the locomotion subsystem, thresholds shall be established for specific sensors. The goal of these thresholds is to allow for normal behavioral variations while at the same time reliably indicating the presence of a fault. Therefore, they need to be higher

than baseline measurement values but low enough to trigger an alarm before causing structural damage to the rover or sensors.

For this signal-based detection method, it is thus necessary to investigate the behavior of the subsystem in its baseline as well as in its different fault states. Only the comparison of the sensor measurements during these different states allows for an appropriate threshold to be determined for the different sensors. For this reason, experiments have to be carried out to enable a thorough understanding of the subsystem's behavior. The maxima of the signals from a fault-free system can be analyzed and compared to those of a faulty system state. The comparison of these values facilitates the definition of an appropriate threshold for each variable, that shows changes in behavior in the comparison. The thresholds are then ideally set within the range of measured fault values but outside the range of the recorded baseline values. This ensures a minimal amount of false positive alarms while ruling out structural damage at the same time. Figure 12 shows the approach to establish thresholds, which differentiate between no fault and fault scenarios on live sensor measurements.

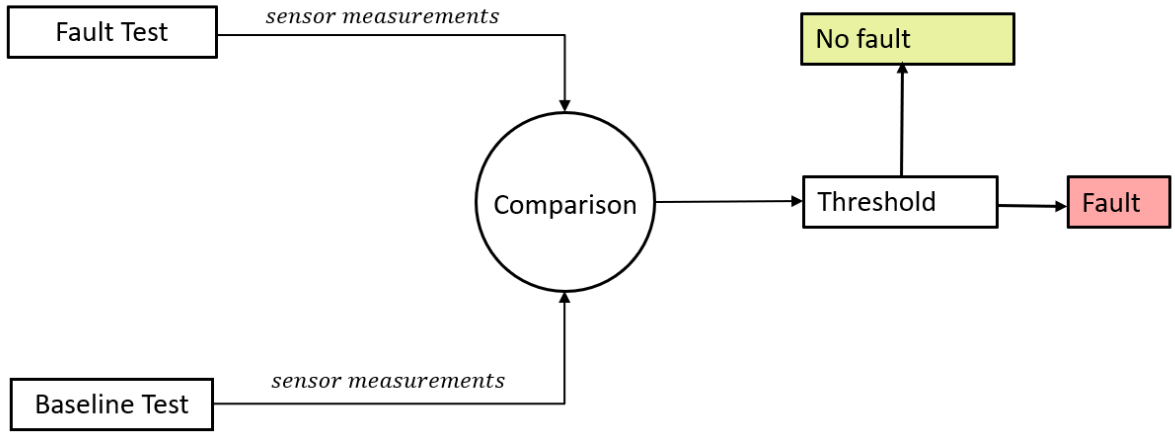


*Figure 12: Fault detection thresholds*

In the case of no fault being detected, the locomotion system remains running, in the event of a fault, the system is shut down to avoid damage and the task of isolating the possible fault ensues.

## 4.2 Data-driven Approach for Fault Identification

For the task of fault isolation, a data-driven approach is taken. The main goal of this step is, as mentioned before, to isolate which fault scenario is affecting the subsystem. For this purpose, measurement samples on all known faults have to be gathered. The symptoms of each fault (a series of values from the measurement data) are then used to train a machine learning algorithm that is based on the principle of logistic regression. This implies that faults are experimentally identified through the subsystem's features and stored in what Isermann [30] calls an "explicit knowledge base". Therefore, known faults can be recognized by observing the

subsystem’s behavior patterns in the future. Once trained on the known fault scenarios, the algorithm now works as a classifier that utilizes the historic data from testbench experiments to determine the current fault scenario based on the subsystem's past behavior patterns.

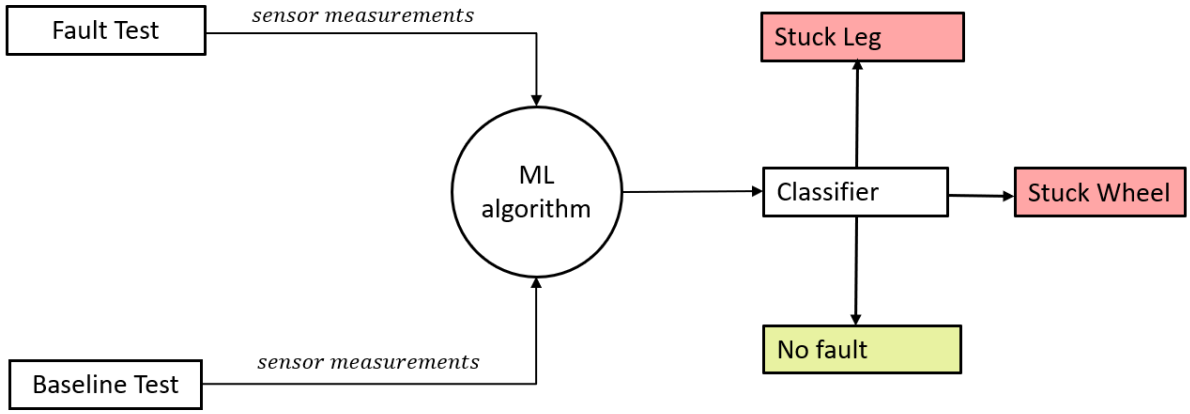


*Figure 13: Fault isolation classifier*

Figure 13 illustrates the basic principle of the fault isolation approach proposed for the MMX rover in this study. All sensor measurements from baseline, as well as fault tests are collected and used to train a machine learning algorithm, which is based on logistic regression.

Logistic regression is a suitable model for the given multiclass classification problem due to its ability to handle linear relationships, provide probabilistic predictions, and offer computational efficiency. By leveraging the linear associations between variables, logistic regression allows for accurate predictions for multiple classes while providing insights into the impact of independent variables. The resulting classifier is then able to differentiate between the fault scenarios of a stuck leg, a stuck wheel or simply variations in normal operation.

# 5 Experimental Verification

To successfully be able to implement these fault detection and isolation methods, and provide reliable safety measures for the system, a few considerations have to be taken into account. Firstly, it is evident that for a threshold to accurately differentiate between slight deviations in the normal behavior and an actual stuck fault, it is necessary to thoroughly understand the baseline characteristics of the locomotion subsystem and define the possible influence of operating and environmental parameters on the sensor measurements. If the measurement values of the sensors show a different behavior for changed parameters, the fault detection threshold have to be adjusted accordingly, depending on the operating conditions and parameters. A series of these must therefore be investigated for their possible impact on the sensor readings before the thresholds can confidently be set. These baseline tests are conducted first to gain knowledge about the subsystem's behavior under normal operating conditions. During these tests no external force or obstacle is applied.

Subsequently it is also necessary to gain knowledge of the impact an applied obstacle has on the sensor measurements. This is essential, as otherwise a clear distinction between normal operation and a stuck fault scenario cannot be reliably established. Additionally, there is a question about how the position of the blockade impacts the measurement values. This aspect is of particular interest, especially with regards to the task of fault isolation.

In order to clarify the impact of these and other parameters on the locomotion subsystem, and thereby tailor and verify the FDI methodology, experiments are conducted on a specifically designed testbench. This chapter expounds upon the parameters subjected to investigation and outlines the execution of the experiments aimed at assessing their influence.

## 5.1 The Testbench Setup

A customized testbench created at the DLR OP (Oberpfaffenhofen) site is used for the conduction of these experiments. The setup consists of one side panel of the rover body chassis with one locomotion unit mounted on an interface frame in a horizontal setup (see schematic in Figure 14).

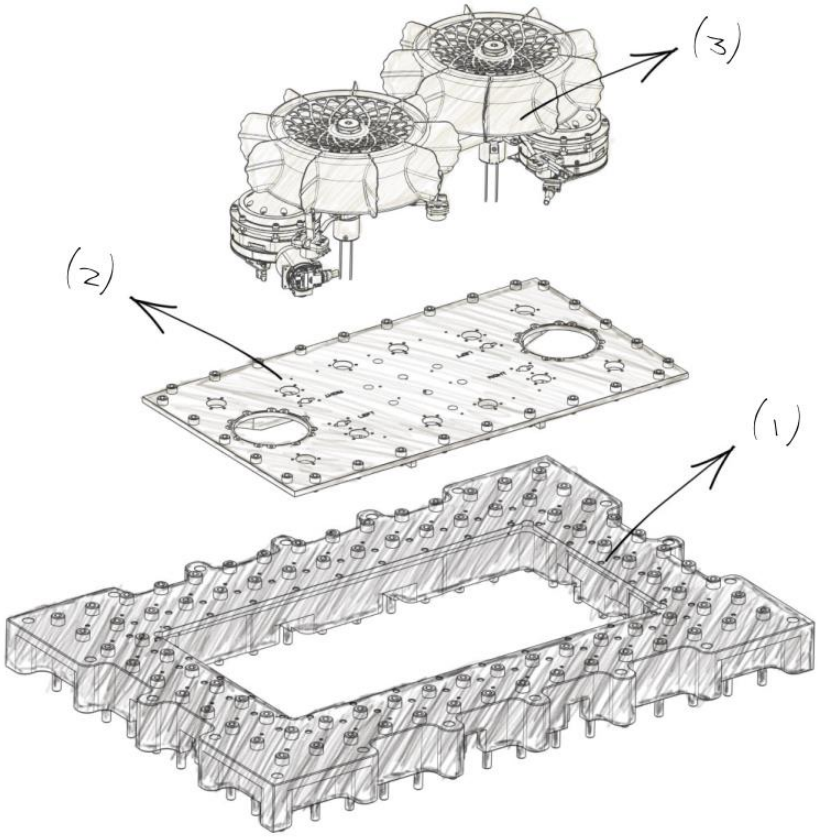


*Figure 14: Setup of the testbench hardware –interface frame (1), chassis side panel (2), locomotion unit (3) [26]*

The unit's motors are controlled, and the sensors read through the Electronics-box (E-box), which is in turn connected to a computer through a Spacewire-to-USB connection and also to the power supply. The PC provides the possibility to command the movements and retrieve the data from the sensors. The E-box is the interface between the software that controls the MMX rover and the physical interaction with the environment that takes place through the mechanical chassis components as well as the sensors. It also includes the motor controller, on which fault detection thresholds can be set on sensor measurements. The power supply provides the E-box with a constant voltage to power the motors.

On the testbench the leg of the locomotion unit can be replaced at the shoulder joint by a low weight 3D-printed alternative. Figure 15 and Figure 16 show the setup of the testbench with, and without the leg of the rover attached.

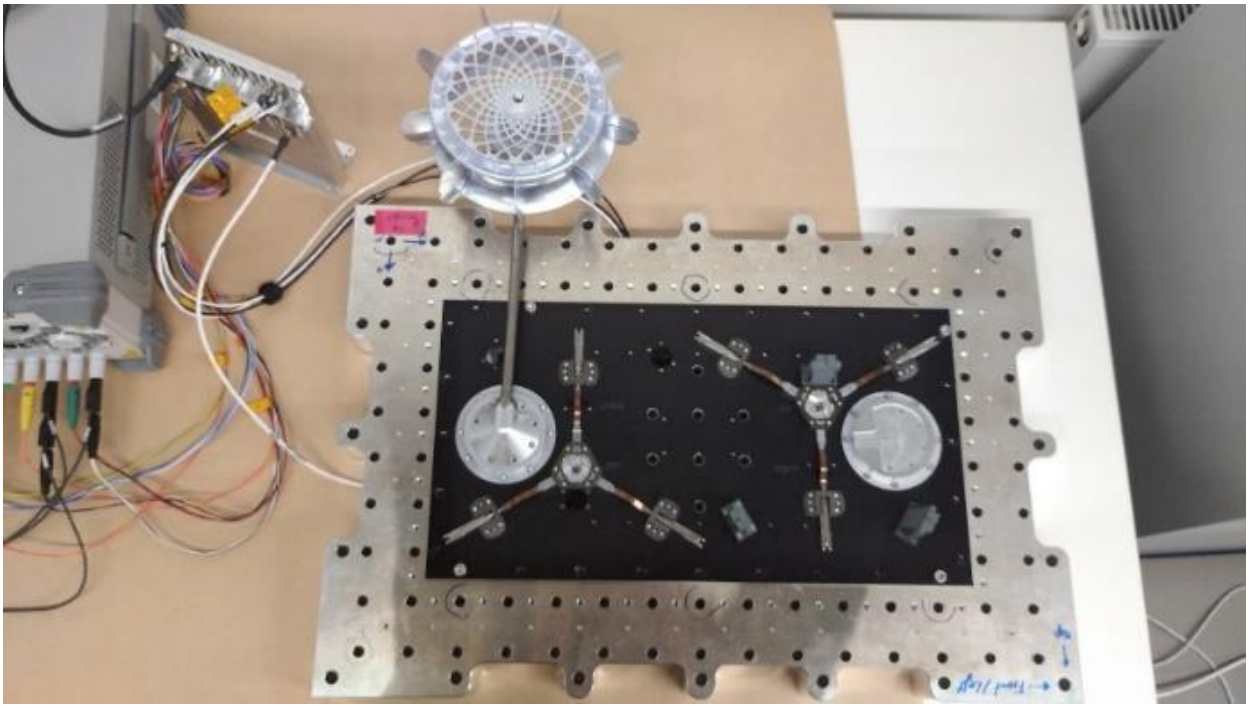

*Figure 15: Testbench setup with leg*

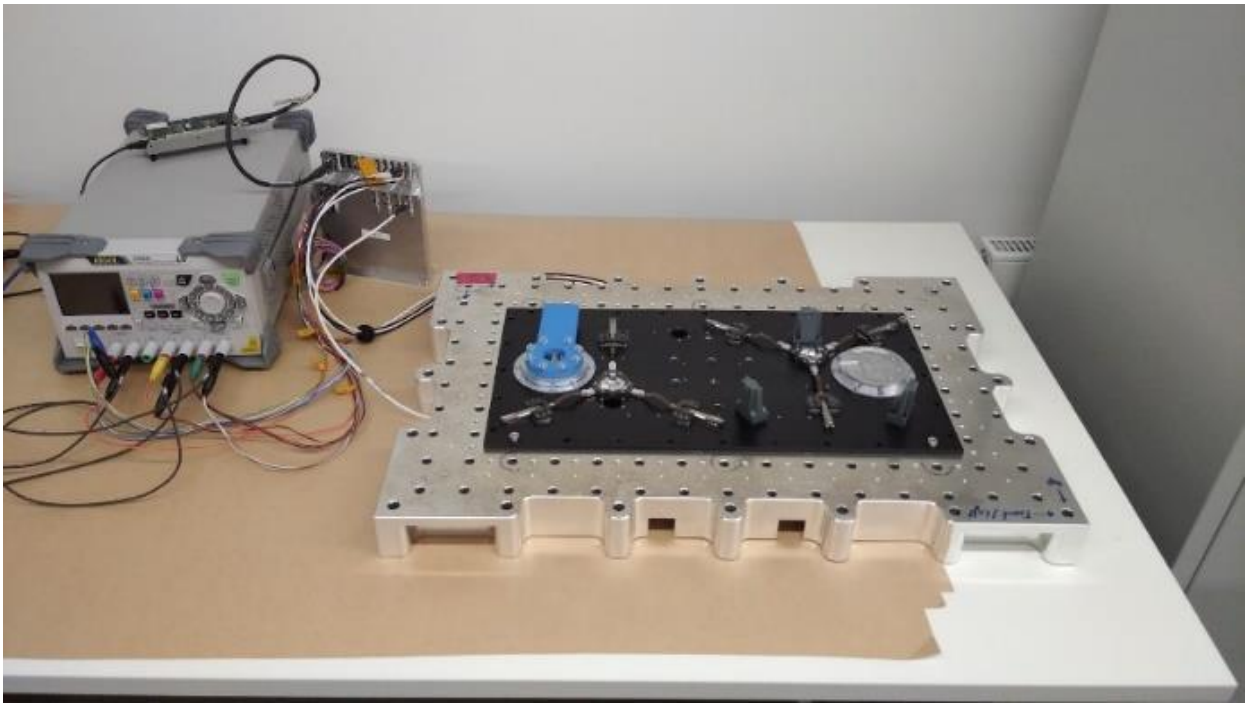

*Figure 16: Testbench setup without leg*

The torque sensor in use on this testbench is built for low torques in the range of $\pm 2\ \mathrm{Nm}$. The mechanical structure of the locomotion unit can withstand higher forces, but it, too is built for very low forces and torques during operation. It is therefore strictly necessary to protect the sensor, and also the structure of the unit, from too high torques and forces during the experiments. Two safety measures are put into place to ensure an end of the test, if stresses become too high.

The first safety measure is to ensure a motor shutdown if current thresholds are exceeded. Secondly, the obstacle is constructed in a fail-safe way. Figure 17 shows the setup of the obstacle, which is used to investigate the influence of the obstacle position on the sensor measurements by itself (on the right) and in use during the simulation of a stuck leg scenario (on the left). To ensure that it does not exert forces higher than allowed on the structure, a click-type torque wrench is used, which can be adjusted to maintain the releasing torque at $2\ \mathrm{Nm}$. The torque wrench is fixed in a metal structure, which can then be clamped to the table in the desired position.

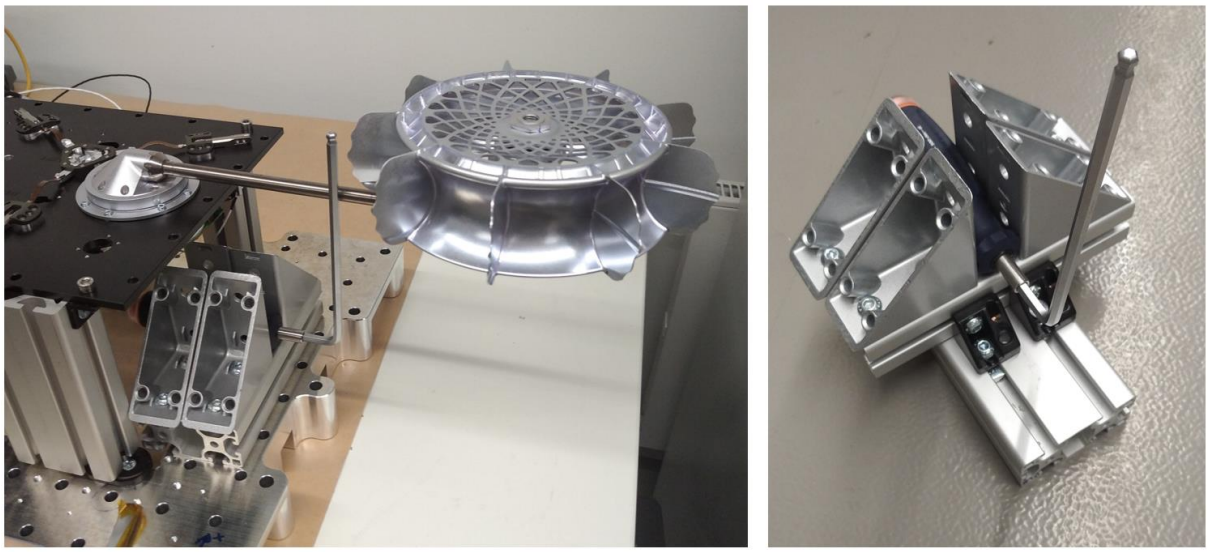

*Figure 17: Obstacle*

## 5.2 Experiment Parameters and Conduction

Several different parameters' influences are investigated through experiments. These parameters include the operational settings of the speed of rotation and the direction of rotation of each of the motors, as well as the parallel operation of both motors simultaneously. External parameters that are expected to have an influence on sensor measurements are the Earth's gravity and the existence and positioning of a potential obstacle, blocking movement of the locomotion unit.

For every experiment parameter setting at least five sets of measurements are created, to ensure comparability and diminish statistical errors in the collected data. For the purpose of

training the machine learning algorithm to work as a most efficient classifier of the different fault scenarios, different parameters are also combined during experiments to provide a wider scope of the collected data.

### 5.2.1 Direction of Rotation

The first operational parameter that is expected to have a potential influence on the measurements of the sensors is the direction of rotation of the two motors, namely clockwise (CW) and counterclockwise (CCW) direction. If the measurements of motor current and torque are dependent on the rotational direction of operation, fault detection thresholds would also have to be set differently for the two different operating modes. Experiments are therefore carried out, in which only the parameter of direction is altered. The tests are repeated at various other parameter settings to make sure that the observations hold true in all scenarios.

### 5.2.2 Speed of Rotation

Secondly, the operating speed of the motors is a parameter that is expected to have an influence on the motor current measurements. Also, a possible impact on the torque measurements has to be studied, to adjust thresholds for each sensor, if necessary.
The brushless DC motor, used in both the shoulder and wheel joint, shows a linear dependency of the current $I$ to the speed $\omega$. Since voltage $U$, torque $M$ and friction $F$ can be assumed as nearly constant, the relationship between ω and I can be seen as linear, as shown in ( II ).

$$\omega = I \cdot \left(\frac{U}{M} + F\right) \qquad \text{( II )}$$

By moving through individual working points of the systems and simultaneously measuring the currents, the function describing the dependency can be obtained. Experiments are conducted at three different speed settings, shown in Table 1. During these tests not only the current but also the torque measurements are recorded and analyzed for possible dependencies.

*Table 1: Rotational speed settings*

| low | medium | high |
|---|---|---|
| $0.01\ \frac{\text{rad}}{\text{s}}$ | $0.03\ \frac{\text{rad}}{\text{s}}$ | $0.05\ \frac{\text{rad}}{\text{s}}$ |

### 5.2.3 Inter-motor Influences

Additionally, the measurements of the sensors with both motors operating in parallel are examined to investigate their potential effects on each other. A simultaneous activation could lead to a drop in voltage and therefore decreased current measurements or an increase in

friction and therefore measured torque due to the mechanical coupling of both joints. Both motors need to operate in parallel for various movement modes of the MMX rover, such as alignment, inching, and uprighting, which require simultaneous activation of shoulder and wheel joints. To rule out an influence between the two drives, experiments are carried out, in which a parallel operation is commanded and compared to measurements at the same parameters with single operation of only one motor.

### 5.2.4 Gravity

The testbench is designed to represent the actual operating conditions during operation as closely as possible. However, the target location of deployment on Phobos represents a milli-gravity environment (0.0057 $\frac{\mathrm{m}}{\mathrm{s}^2}$ [31]), which cannot be reproduced on Earth. To minimize the effects of the existing gravity, the testbench is set up in a horizontal orientation. To investigate the influence of the leg's weight acting on the mechanics because of the horizontal setup under Earth gravity conditions, the leg on the testbench can be replaced by a low weight 3D-printed module. The reduction of weight is expected to lower friction in the system, which leads to a decreased current and torque measurement. To investigate the impact of this parameter on the measurements, a comparative analysis is performed. In one set of experiments, the leg is replaced with a 3D-printed placeholder that has only around one tenth of the original weight. This allows for a direct comparison between the measurements obtained with the original leg and the low-weight alternative.

### 5.2.5 Location of Obstacle

The most important parameter for the task of fault detection and isolation is the existence and location of an obstacle in the path of movement of the locomotion unit. The encounter of an obstacle represents the faults that are of interest in this thesis. The investigation of the influence on the measurements of not only the existence of an obstacle, which provides necessary insight into the differences to be expected between normal operation under varying operating conditions and a stuck fault scenario, but furthermore of the location of the obstacle, which is indispensable for effective stuck fault isolation, presents the cornerstone to aligning and validating the proposed fault detection and isolation methodology.

Various experiments are carried out to simulate the different expected fault scenarios and be able to compare them to baseline tests, with no external blockade. A schematic representation of the difference in positions of obstacle encounter is shown in Figure 18.

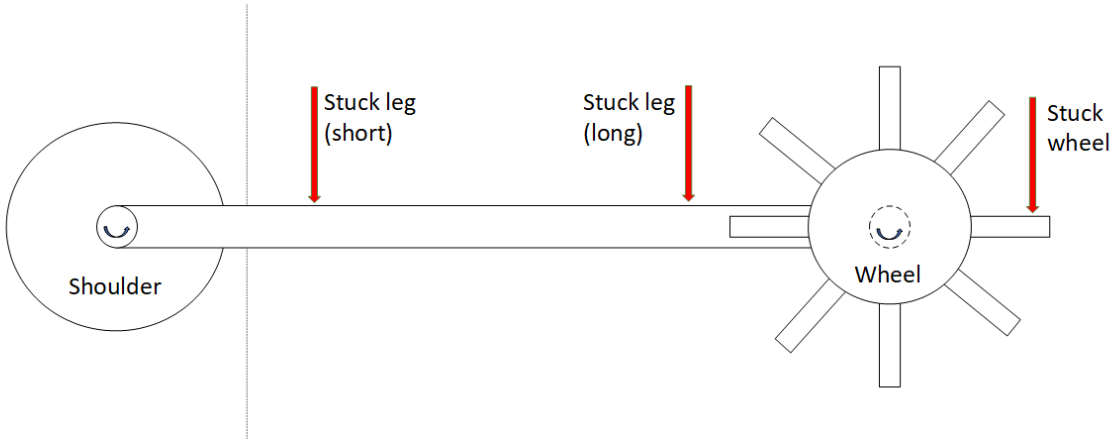


*Figure 18: Tested fault scenarios*

The stuck leg scenario is simulated at two different positions: a short distance of 9 cm where the leg shaft encountered an obstacle near the shoulder rotation axis, and a further distance of 16cm down the shaft. Additionally, experiments are also carried out where one of the wheel grousers is jammed by the obstacle, directly in line with the leg axis. These experiments allow a comparison of fault scenario measurements with the baseline operation data, in addition to an investigation into the different behavior of the system through a change in location of the fault.

# 6 Data Analysis and Discussion

This chapter presents the outcomes of the experiments described in section 5, along with an analysis of the implications these findings hold for the suggested FDI methodology. Moreover, a discussion regarding the implementation and overall effectiveness of the fault detection and isolation system is presented.

## 6.1 Irregularities in the Torque Sensor

The torque sensor is located inside the shoulder module and is therefore also influenced by friction between gears and bearings. Therefore, no qualitative but only a quantitative statement can be made about the measured torque values. To still be able to interpret the values measured, defined torques are exerted onto the leg and the measured torque is recorded at the same time. The force is applied at a defined distance of 20 cm in a perpendicular direction to the leg with a spring scale. The torque is then increased in $0.5\ Nm$ intervals up to $2\ Nm$, first in counterclockwise, then in clockwise direction. The measurements recorded during that test, are shown in Figure 19.

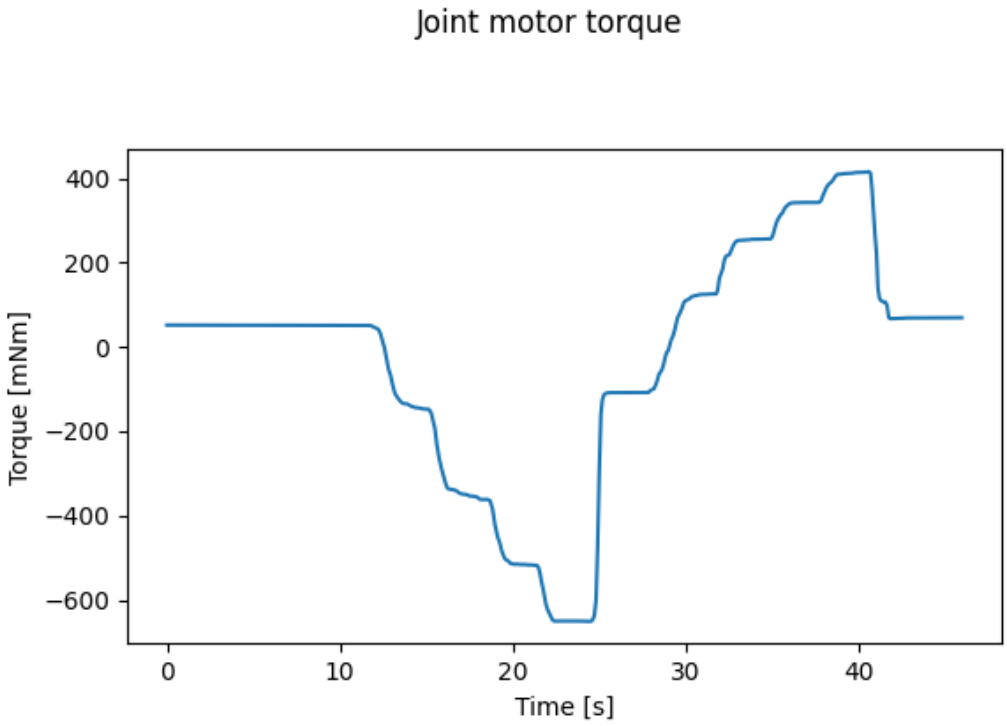


*Figure 19: Torque sensor sensitivity*

The course of the graph shows a significant reduction of the measured torques compared to the exerted ones. It is also visible that the sensitivity of the sensor is lower in clockwise than in the opposite direction. The size of the steps also decreases at higher moments, showing

that the sensor is subject to saturation. With the aim of setting a threshold on this value for fault detection, it must be ensured that the thresholds do not fall outside this measuring range.

## 6.2 Correlations and Dependencies in the Sensor Measurements

Through experiments, the influence of several parameters is assessed. Possible dependencies of the sensor measurements, on which thresholds shall be set to detect faults, on the parameters have to be studied and, if needed, taken into account for setting reliable thresholds. The baseline tests, where no obstacle is applied, aim to evaluate the impact of speed and direction of rotation on sensor measurements, particularly on the motor currents and torque. Additionally, the measurements with two motors operating in parallel are examined to investigate their potential effects on each other. Furthermore, the influence of the weight of the leg structure on sensor measurements is explored.

### *Impact of the commanded rotational speed and direction*

The first area of interest is the behavior of the current and torque measurements depending on the rotational speed and direction of rotation of the motor under examination. Several noteworthy observations can be made from the collected measurements. Firstly, it can be noted that the measured motor current exhibits a linear relationship with the commanded rotational speed. This proportional correlation held true for both directions of rotation and can be observed in Figure 20.

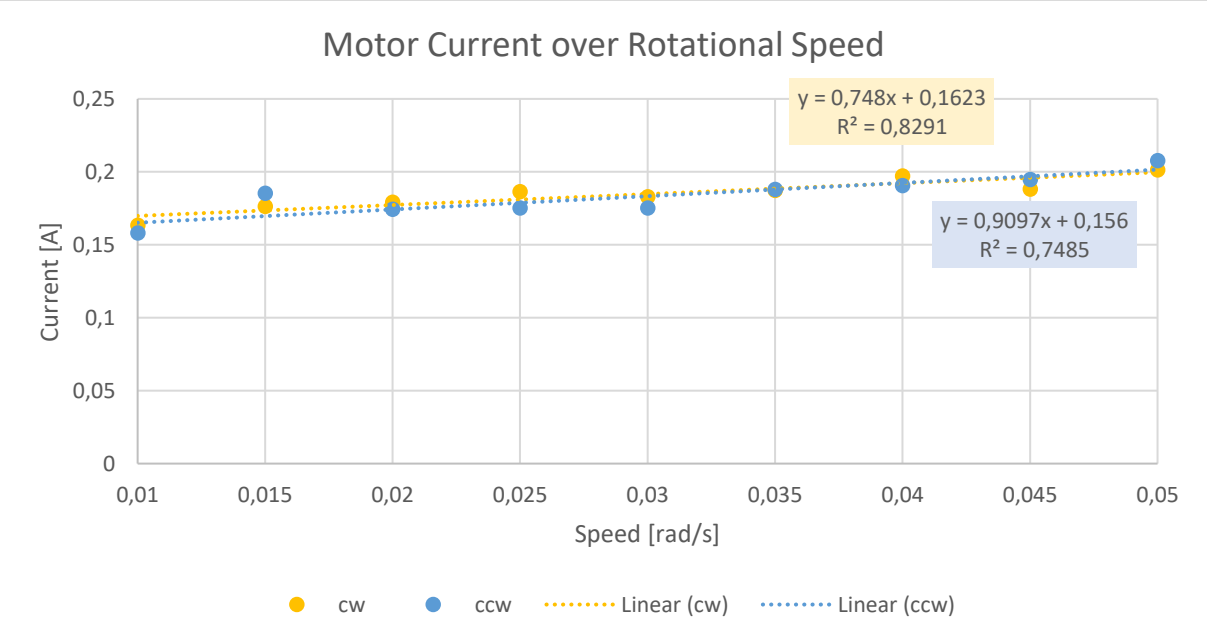


*Figure 20: Linear relation between current and speed*

This linear dependency of the current on the rotational speed is in accordance with the expectations presented in chapter 5.2.2. A slight difference can be observed between the clockwise and counterclockwise measurements, but the magnitude of this difference is smaller than the

variance of the measured values. In summary it can therefore be concluded that while the current is dependent on the speed, a change of the direction of rotation does not significantly alter the motor current.

Secondly, it can be noted from the variations of speed and rotation direction in the experiments, that the measured torque, equal to the current, slightly increases with a gain in rotation speed (see Figure 21). This is due to higher friction in the mechanical parts at higher levels of rotational speed. Additionally, a change in direction alters the sign of the measurements, with generally lower amplitudes in counterclockwise test cases compared to their clockwise equivalents. This relationship can also be seen in Figure 21.

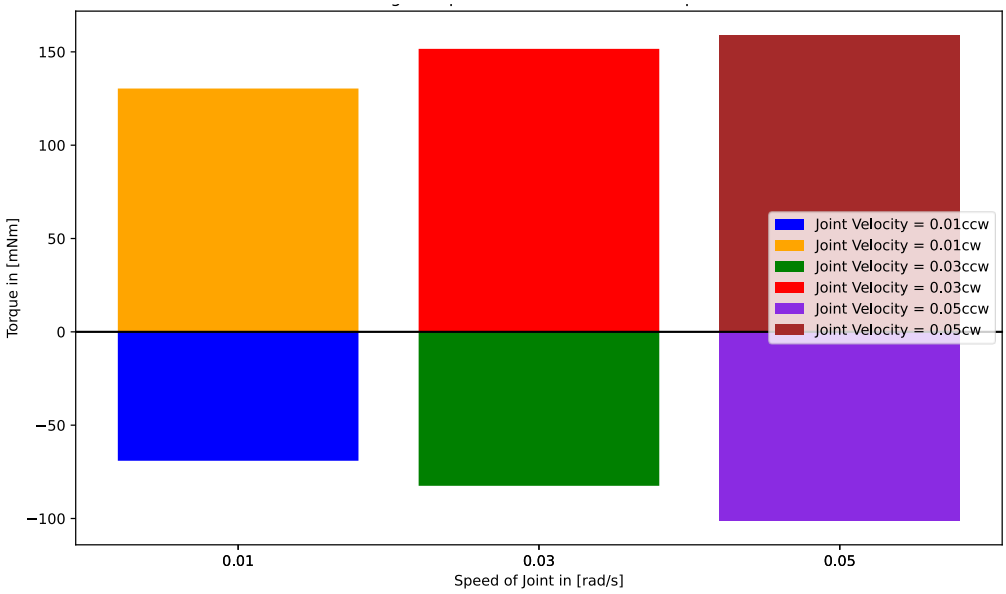


*Figure 21: Average torque for different shoulder speeds*

## *Inter-Motor Influences*

Another parameter of interest is the potential mutual influence between the two motors in the rover locomotion unit. Both drives need to operate in parallel for various movement modes of the MMX rover, such as alignment, inching, and uprighting, which require simultaneous activation of shoulder and wheel joints. The next question to be answered is therefore whether the current or torque of one motor is influenced by the activation and operation of the other motor. The results of the experiment investigating the system's behavior for a change in this parameter can be observed in Figure 22.

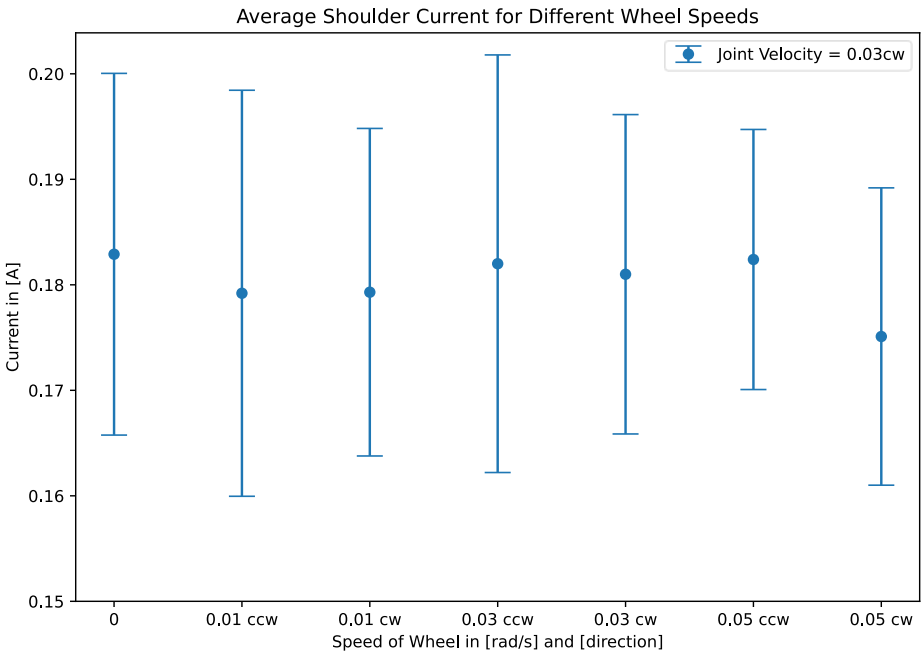


*Figure 22: Average shoulder current for different wheel speeds*

Figure 22 shows the average current of the shoulder motor along with its standard deviation for the seven different operation modes of the wheel motor. No change in parameter on the shoulder motor is conducted over the course of these experiments. The shoulder motor current shows no drop or other non-statistical change across the various experiments, indicating that the activation or operation of the wheel motor does not influence the current measurements of the shoulder motor. Likewise, the same effect is observed in the opposite direction: the activation of the shoulder motor does not impact the wheel motor, as can be seen in Figure 23.

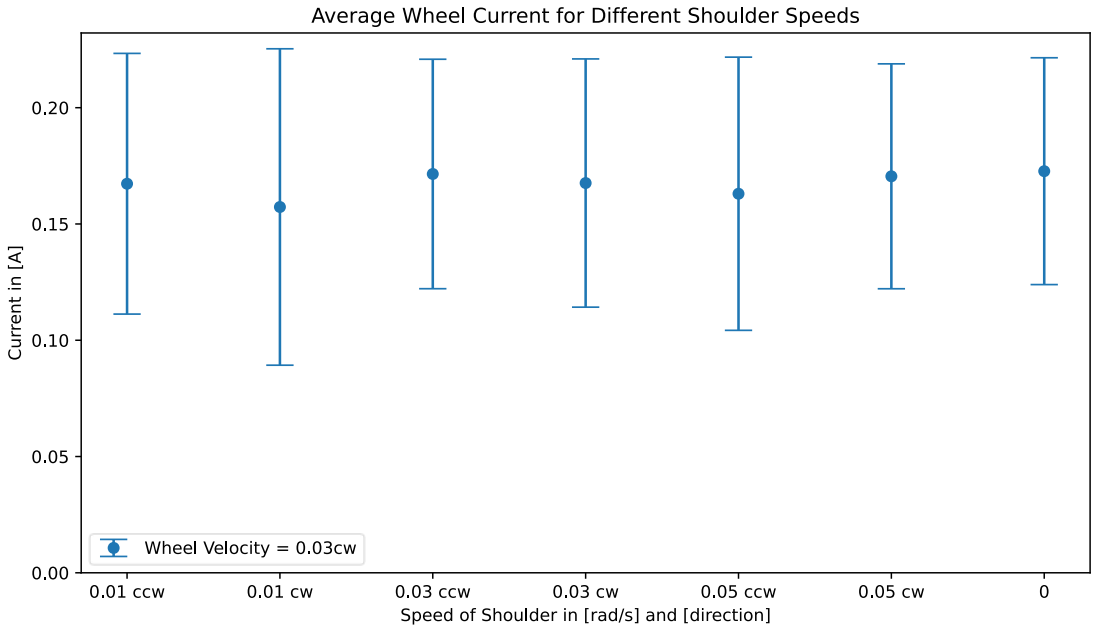


*Figure 23: Average wheel current for different shoulder speeds*

In the same manner as the motor currents, the torque measured on the shoulder joint remains independent of the speed or activation of the wheel motor. In Figure 24 the average torque of the shoulder motor for different speed and direction parameters of both motors can be seen. All points of a single color represent constant parameters of the shoulder motor, while different colors represent different speed and directions on the shoulder drive. On the horizontal axis, the modes of the wheel motor can be seen. While there is no trend visible in the horizontal direction for any color (therefore no dependency of the torque on the other motor), the stacking of the colors represents the dependency of the torque on the speed and direction of the same motor as mentioned before.

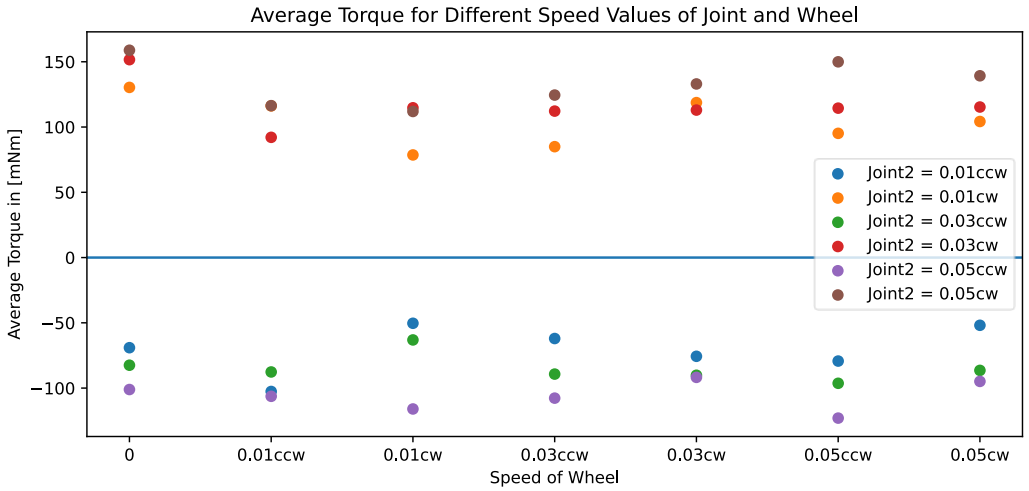


*Figure 24: Average torque of the shoulder motor*

## *Influence of gravity and the weight of the leg structure on the shoulder motor*

Lastly, the influence of the weight of the leg structure in Earth gravity on the measurements of motor currents and torque is examined. The result of the comparative analysis is shown in Table 2. “No leg” represents the experiment set with the low weight 3D-printed module, while “with leg” refers to the set of experiments with the original leg of the locomotion unit attached. The direct comparison between the two sets of tests shows that both the current and the torque sensor show lower measurement values with the weight of the leg removed, while the standard deviation (SD) remains virtually unchanged. The current decreases by around 2%, the torque by almost 8% in its mean value.

*Table 2: Influence of the leg structure on the measurements*

| | **Mean Current** | **Mean Torque** | **SD Current** | **SD Torque** | **Difference in Mean Current in %** | **Difference in Mean Torque in %** |
|---|---|---|---|---|---|---|
| **No leg** | 0.179 A | 139.9 mNm | 0.0116 A | 33.78 mNm | - 2.2 | - 7.7 |
| **With leg** | 0.183 A | 151.6 mNm | 0.0171 A | 38.32 mNm | | |

These decreases are shown in more detail in Figure 25 and Figure 26

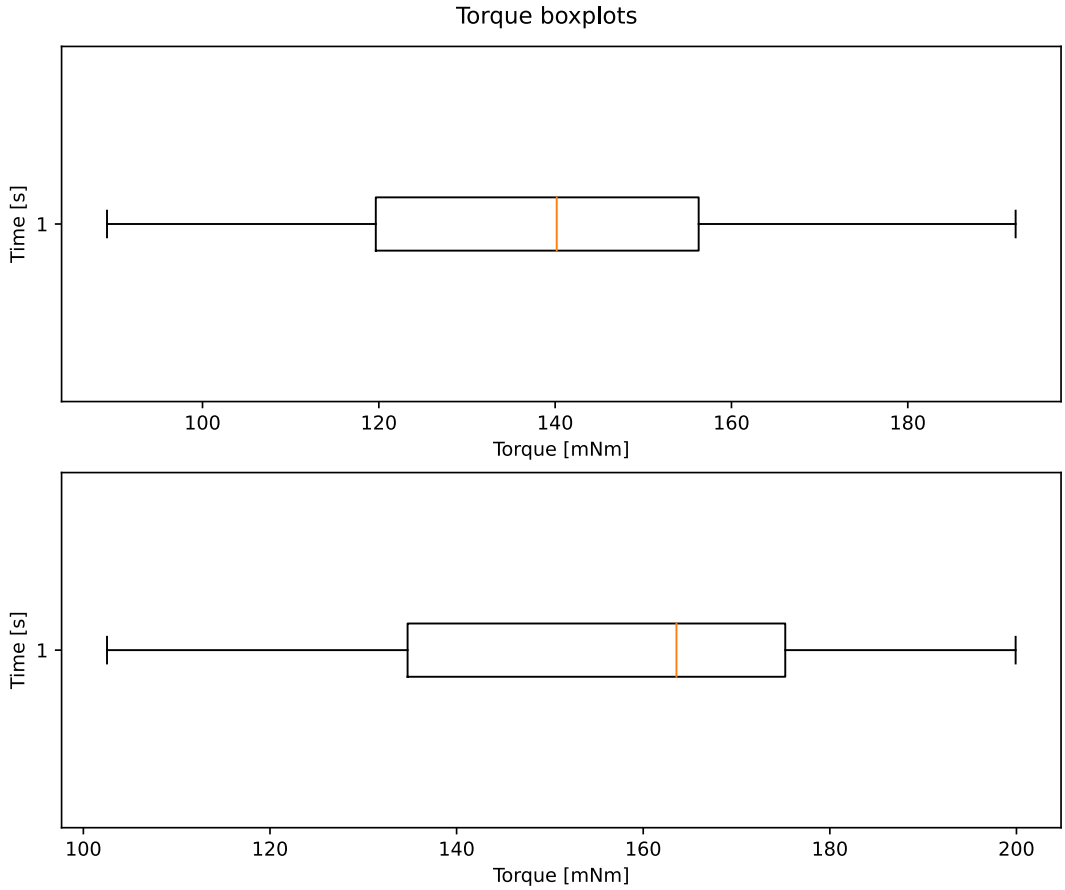


*Figure 25: Shoulder torque with (down) and without (up) leg structure*

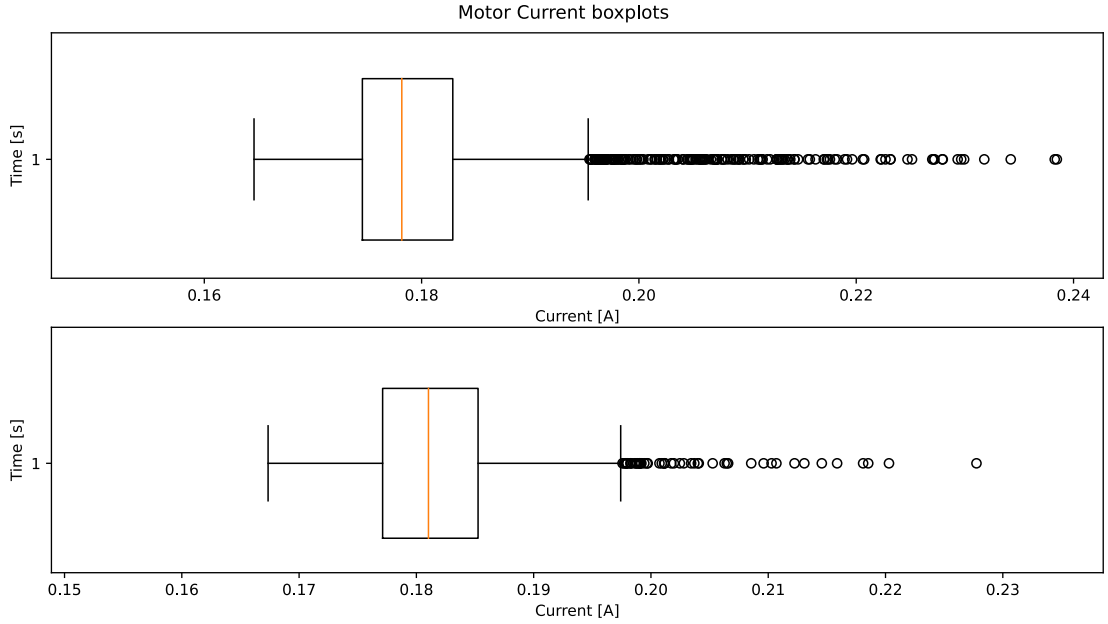


*Figure 26: Shoulder motor current with (down) and without (up) leg structure*

This finding suggests that the weight of the leg structure in Earth gravity introduces anticipated deviations and distortions in the measured data, compared to the expected conditions on Phobos. Since the values are higher when using the attached leg structure, the thresholds to detect

faults in these sensors need to be reduced by the mentioned above percentage to pertain the same effect. Despite the influence of gravity on this testbench, the experimental setup involving the horizontal configuration still provides the most accurate reflection of the unit's behavior under the low-gravity condition of Phobos.

### *Oscillation of the torque during wheel movements*

The presence of oscillations in the torque measurements when only the wheel motor is activated is observed during the experiments. An exemplary timeline of torque and current measurements where this can be seen is given in Figure 27. The frequency of these oscillations corresponds to the rotation frequency of the wheel drive train before the last gear stage. The small peaks visible along the curve correspond to the number of teeth on the gearwheel driving the crown gear. This indicates that the oscillation is caused by an imbalance in the wheel resulting in a change in torque, dependent on the position of the wheel. Small torque peaks are also visible, which represent the additional torque during the meshing of the gear teeth.

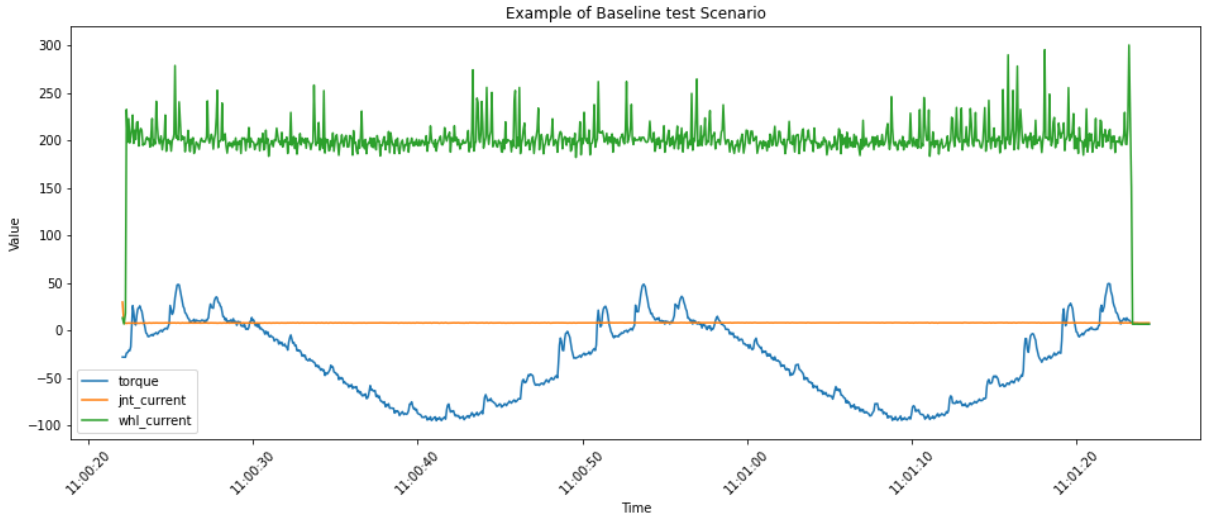


*Figure 27: Torque oscillation*

### *Influence of the obstacle on the sensor measurements*

The boxplots shown below in Figure 28 depict all maximum values recorded during clockwise baseline testing (144 tests) and fault testing (255 tests). The left figure shows the boxplot of all torque maxima that are reached during clockwise baseline testing. It can be noted that the maximum value is at $T_{max} = 230.6\ \mathrm{mNm}$. In the same boxplot for clockwise fault scenarios, shown on the left, the maximum torque exceeds $450\ \mathrm{mNm}$. As expected, an external application of an obstacle does therefore lead to a significant increase in torque.

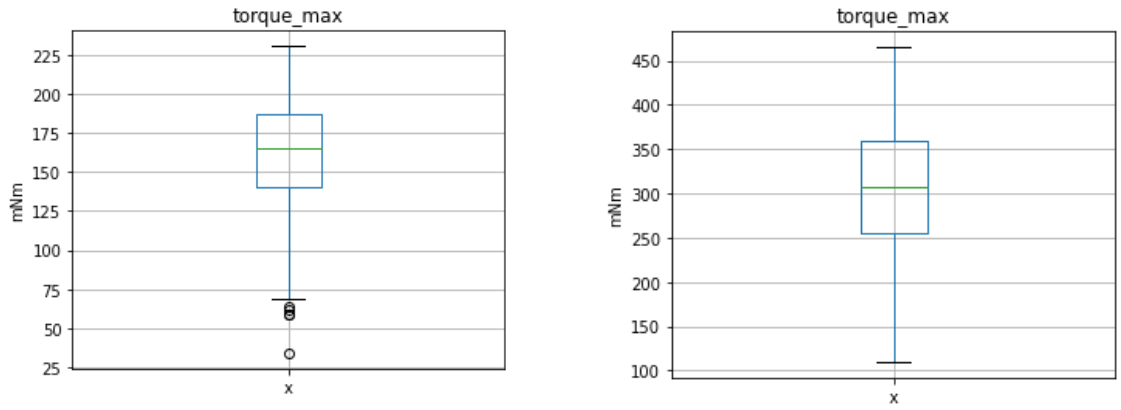


*Figure 28: Torque maxima reached during baseline (left) and fault testing (right), clockwise direction*

The same effect is visible in the counterclockwise torque measurements (see Figure 29). However, in this case, the minima have to be evaluated, since the torque is measured below zero during counterclockwise motion. It is shown that the minimum value reached is at $T_{min} = -230.8\ \mathrm{mNm}$. In the same boxplot for the counterclockwise fault scenarios the minimum torque falls below $-600\ \mathrm{mNm}$.

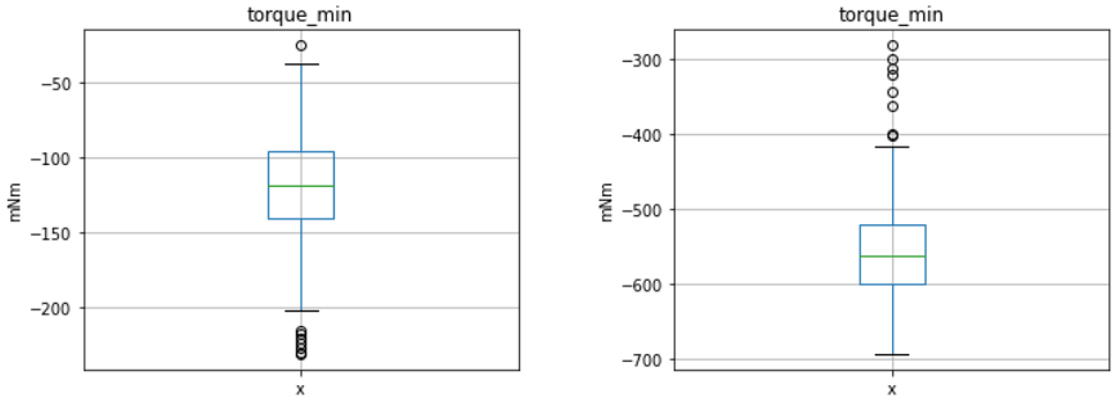


*Figure 29: Torque minima for baseline (left) and fault (right) testing, counterclockwise*

Figure 30 shows the maximal measurements values of the shoulder motor current during baseline tests and fault tests. Here it can be seen that there are outliers in the maximal currents due to oscillations, caused by high noise on the current sensors. Even though the outliers are at around the same level, it is shown in the boxplots, that on average, the maximal current is higher during fault testing, than during experiments with no obstacle placement.

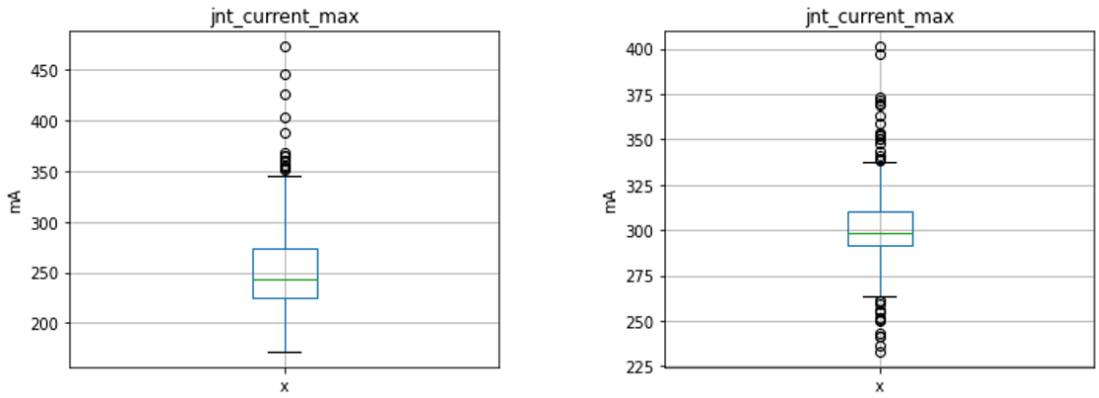


*Figure 30: Shoulder motor current maxima during baseline (left) and fault (right) testing*

Figure 31 shows the maxima of the wheel current sensor during fault-free and fault scenario testing. Even though the average maximum current is lower in the experiments with an obstacle, the boxplots do show a higher maximum current reached during these scenarios compared to baseline tests.

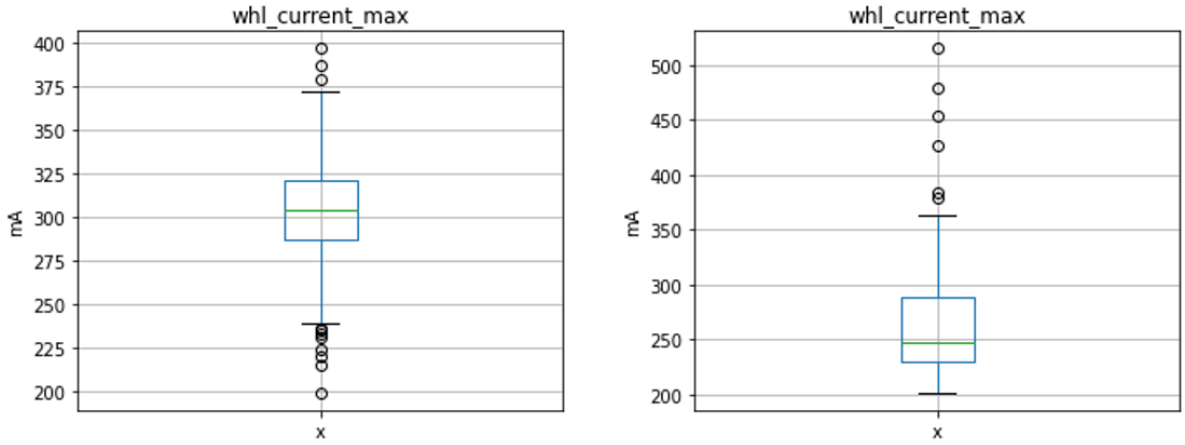


*Figure 31: Wheel motor current maxima during baseline (left) and fault (right) testing*

## 6.3 Consequences for the Detection of a Fault

The detection of a fault by a signal-based method through thresholds on the motor current and torque sensor measurements is reliant on a thorough understanding of the sensors' behavior during changes of parameters. The conclusions drawn from the experiments investigating the influence of certain important parameters consequently have an impact on the design of the thresholds to detect faulty situations. These conclusions and their implications and consequences for the FDI methodology are described more closely hereinafter.

From the experiments that investigate the influence of the parameter of speed it is concluded that an increase of speed increases the motor current as well as the torque sensor measurement values. A threshold on these sensors as per the fault detection methodology would therefore need to be speed dependent or otherwise set higher than the values measured at the highest speed to avoid false alarms. The study of the parameter of rotation direction shows that while the current measurements suggest no significant dependency, the torque sensor switches to negative values for counterclockwise motion and furthermore decreases in value compared to clockwise rotations. This hence requires the torque sensor to have two thresholds installed, one for each direction of rotation respectively. The parallel operation of both motors shows no change in the measurement values, this parameter does therefore not need to be considered for the detection of a fault by thresholds. In comparison, the parameter of gravity does cause a reduction of sensor measurement values. In order to still pertain the same effect, the thresholds need to therefore be reduced by the observed percentage. The oscillations in the wheel torque sensors do not have an influence on the necessary height of the thresholds, since they only occur at non-operation of the shoulder module and are too small in amplitude to trigger a false alarm.

To successfully implement a fault detection system by setting thresholds, the last important parameter to determine the height of these is the presence of a fault and the influence this has on the sensors. If the thresholds are set too low, false positive alarms will unnecessarily halt mission progress. If on the other hand the thresholds are set too high, alarms could be raised too late, potentially after sustaining structural damage or reaching an irrecoverable situation. To find adequate values for the thresholds both data from the baseline tests, as well as all fault scenarios need to be considered. Ideally, the thresholds shall be set higher than the maximum values recorded during all parameters variated in baseline testing, with an additional margin to avoid false alarms, yet lower than the lowest maximum values reached during the fault testing to ensure fault detection in time to rule out structural damage. However, considering the maximum values recorded during testing, summarized in Table 3, it is not possible to set the thresholds by that logic alone, since minimal fault peak measurements are lower than maximum baseline peak measurements. The highest torque peak recorded during the baseline tests $T_{base}$ exceeds the lowest maximum torque peak measured during the fault scenario tests $T_{fault}$. The same effect can be seen with the currents of the shoulder motor $I_s$ and the wheel motor $I_w$.

*Table 3: Maximum values of baseline and fault tests*

| $\max(\max T_{base})$ | $\min(\max T_{fault})$ | $\max(\max I_{s,base})$ | $\min(\max I_{s,fault})$ | $\max(\max I_{w,base})$ | $\min(\max I_{w,fault})$ |
|---|---|---|---|---|---|
| 230.6 mNm | 110 mNm | 473.1 mA | 233.1mA | 397.1 mA | 175.9mA |

To minimize the number of false positive alarms during operation, the thresholds shall still be set higher than the maximum values reached during nominal operation. The nature of a fault

caused by actuator blockage is progressive over time, so a higher threshold results in a delayed detection, rather than a failure to recognize the fault in general. The only limitation to this approach is the potential structural damage occurring after a certain amount of force is exerted on the system. Since no such damage occurred during testing, it is safe to assume that the maxima reached during fault testing are within an acceptable range of current and torque.

The threshold value for the torque in clockwise direction is therefore set to $y_{T,cw} = 240\ \mathrm{mNm}$, higher than the highest baseline torque value at $230.6\ \mathrm{mNm}$. Following the same logic, the threshold value for the torque in counterclockwise direction is set lower than the lowest baseline test minimum to $y_{T,ccw} = -240\ \mathrm{mNm}$ to indicate non-nominal behavior.

Additionally, a threshold for the motor currents has to be set. To avoid setting a threshold that is too low and triggers unnecessary false positive alarms, while also preventing structural damage, the threshold value for the shoulder current is set above the Q3 line in the baseline values, but below the maximum measurements from the fault tests. The recommended threshold for the shoulder current is $y_{jnt} = 360\ \mathrm{mA}$.

To further minimize false positive alarms, the threshold shall be implemented in a way that triggers an alarm only, when the threshold is exceeded by three or more consecutive values. This approach ensures that single peaks resulting from noise are not considered as faults by the system. An example of a single peak in oscillation, causing a breach of the shoulder motor current threshold during a test without fault, is shown in Figure 32.

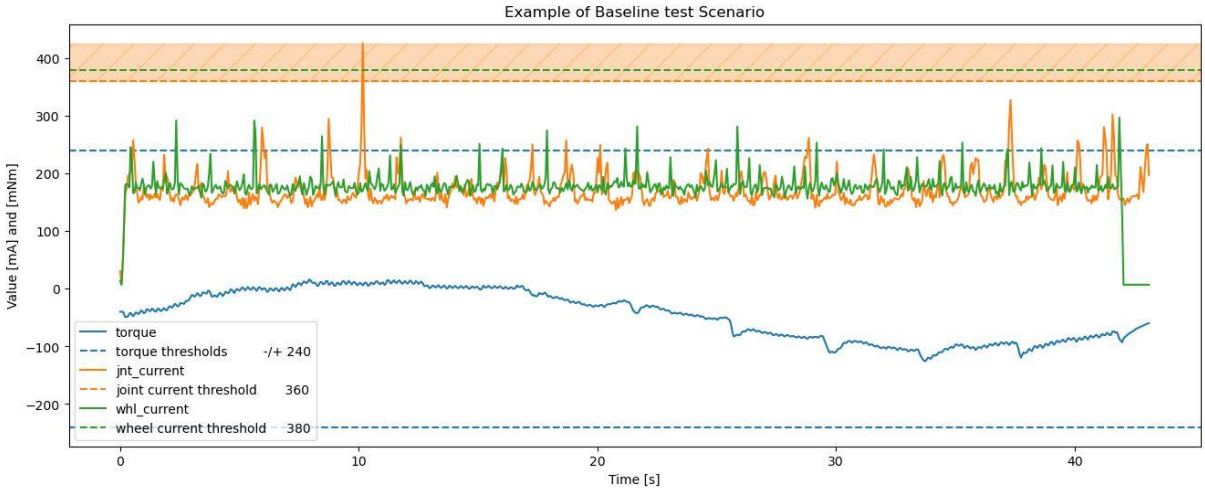


*Figure 32: Current oscillations exceeding the threshold*

The same principle for setting the threshold is applied to the wheel motor currents. The Q3 value of the baseline maximal wheel currents is $373\ \mathrm{mA}$, while the maximum reached during fault testing is $516\ \mathrm{mA}$. The recommended threshold is therefore set to $y_{whl} = 380\ \mathrm{mA}$. Similar to the shoulder current threshold, this limit shall only be triggered by three or more consecutive exceedances to avoid noise peaks triggering false positive alarms.

The defined thresholds in comparison to measurement values are illustrated in Figure 33, Figure 34 and Figure 35 for the baseline, stuck leg and stuck wheel scenarios respectively. It can

be observed that the torque proves to be the most reliable indicator for detecting fault scenarios as it responds the fastest to external loads.

Figure 33 shows the three sensor measurements in three different colors, with their respective thresholds in dotted lines in the corresponding color. In this experiment no obstacle is placed in the path of the leg or wheel and no threshold is exceeded accordingly.

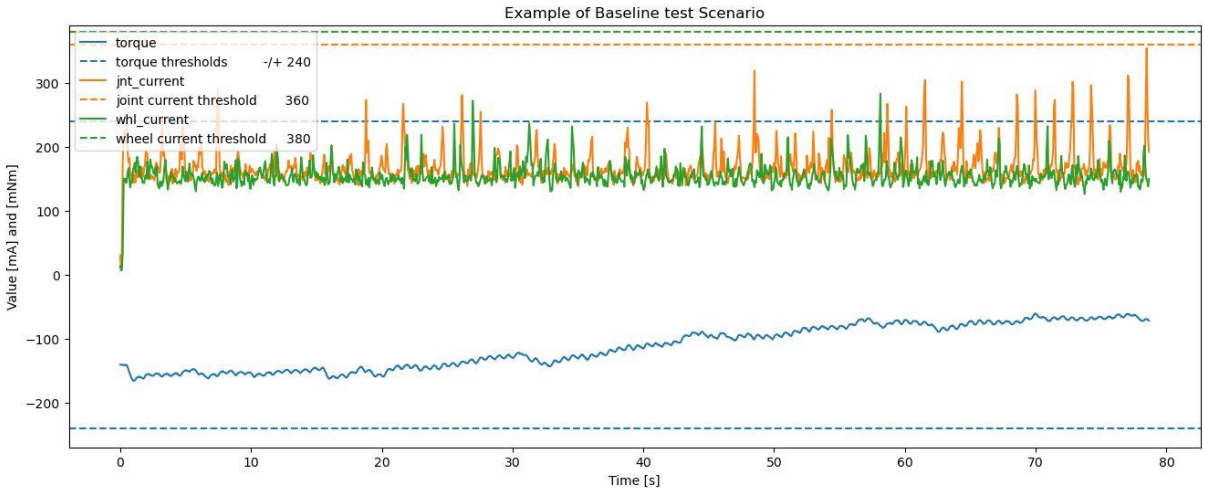


*Figure 33: Baseline with thresholds*

In Figure 34, the shoulder is moved in a counterclockwise motion and the obstacle is placed in the way of the leg, leading to the exceeding of the minimal torque threshold in that graph. The shoulder current also shows a linear rising, although much more subtle.

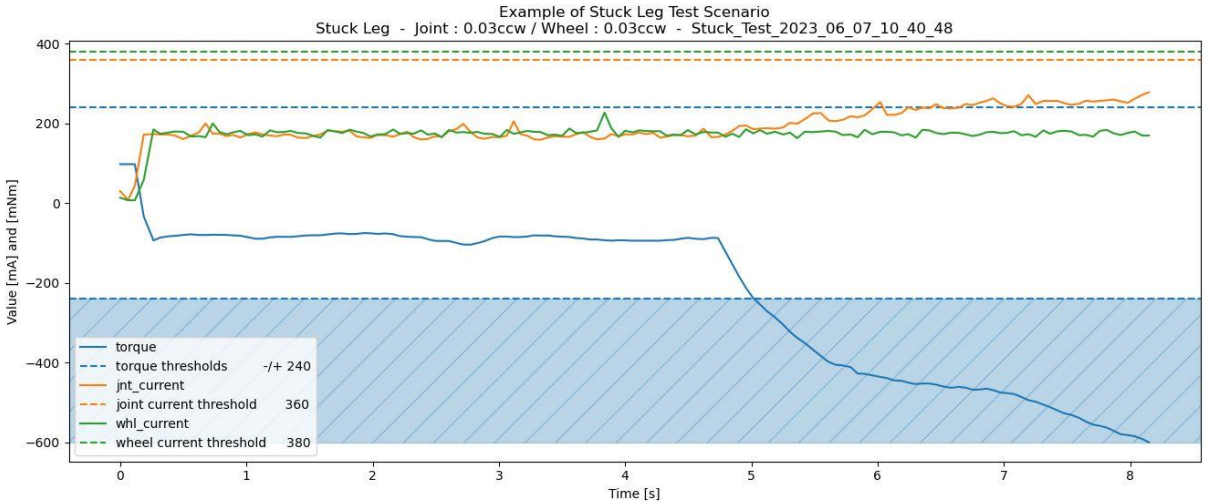


*Figure 34: Thresholds during stuck leg*

Figure 35 depicts the measurements from a stuck wheel experiment. Again, the torque sensor is first in detecting the fault, although both current sensors show an increase that would inevitably lead to an exceeded threshold on both sensors in case the torque sensor does not react.

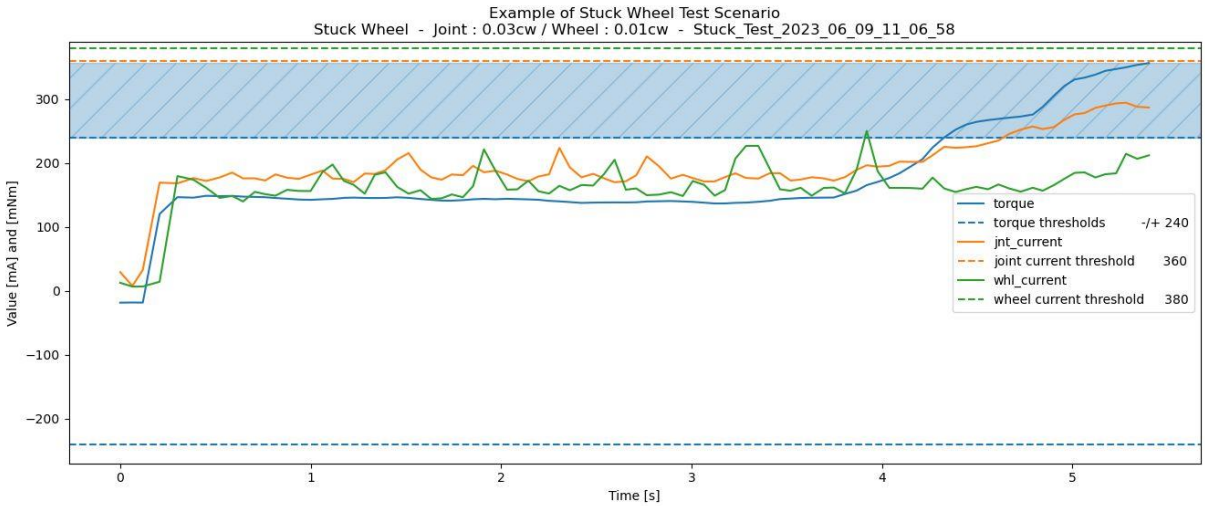


*Figure 35: Thresholds during stuck wheel*

These figures show the effectiveness of the set thresholds in detecting a stuck fault, along with their ability to tolerate oscillations and small deviations in the sensor measurements due to changing operating conditions.

## 6.4 Results on the Differentiation between the Fault Scenarios

Figure 36 shows a graphical representation of the distribution of tests conducted for the different scenarios and parameters to enhance understanding of the collected measurements. In total, equal amounts of every speed and direction setting are tested. The direction label “None” represents a test, where the motor is not operated at all, the same applies for the speed label “0”. In total, more than 800 tests are conducted for the baseline, stuck leg, and stuck wheel scenarios at different parameters.

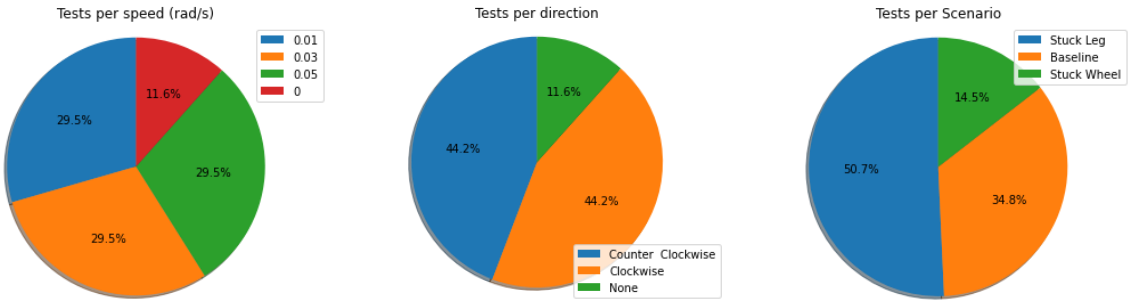


*Figure 36: Test distribution*

The data collected during testing serves as the foundation for identifying a fault’s characteristics and distinguishing between different fault scenarios with the help of machine learning. All test data, including baseline, stuck leg and stuck wheel tests are consolidated into a single master file. This file contains metadata (test type, test parameters) and descriptive statistics of

the test measurements. Subsequently, the master file undergoes processing. During this process any categorical data, such as the direction, is converted into a numerical value to facilitate further processing by the machine learning algorithm. The algorithm used is based on the statistical method of logistic regression, as explained in chapter 2.2.2, meaning it uses the features, such as minimum, maximum or mean values from the input data to determine which of the discrete outcomes: baseline, stuck leg or stuck wheel apply to the specific dataset.
As mentioned before, the algorithm is trained using various characteristics of the test data, including mean, variance, standard deviation, minimum, maximum, median, skewness, and kurtosis. The latter two are explained in Table 4.

*Table 4: Characteristic features of the data*

| Characteristic | Explanation |
|---|---|
| Skewness | Skewness is a measure that assesses the asymmetry or lack of symmetry in a dataset's distribution. It provides information about the extent, to which the data deviates from a symmetrical bell-shaped curve, indicating the presence and direction of skewness. |
| Kurtosis | Kurtosis is a statistical measure that describes the shape of a distribution and provides insights into the tails of the distribution. It quantifies the level of peaked-ness or flatness in comparison to a normal distribution. |

To help the algorithm converge, a scaler is applied to the numerical features. This ensures that every numerical value in the final master file is comprised in a range between -1 and 1. The data is then randomly divided into training and testing sets in an 80:20 ratio. The logistic regression algorithm is then trained on the training set and evaluated using cross-validation on the testing set. The optimal parameters for the algorithm are explored and refined through a grid search where every combination of a finite set of logistic regression hyperparameter alternatives are trained.
The initial analysis shows an 86% accuracy in predicting specific fault scenarios, irrespective of motor speed, direction, or mode combination. The algorithm's performance in identifying the fault is evaluated through the use of a confusion matrix, shown in Figure 37, providing a comprehensive overview of the testing results. The matrix displays the number of correct identifications on the diagonal axis, while all other values represent false predictions. The values in the top row, outside the diagonal, indicate the number of false positive predictions, which were found to be low (three out of 166 or 1.8%), demonstrating the algorithm's ability to correctly identify normal system behavior in the absence of faults.

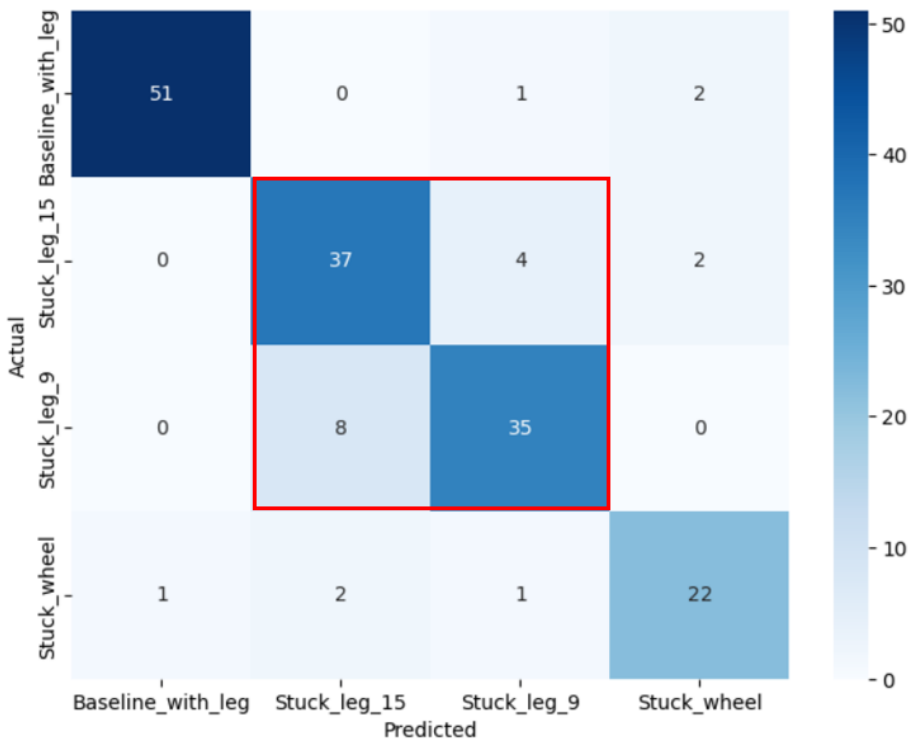


*Figure 37: Confusion matrix*

It is worth noting that the highest number of false identifications occur within the same type of fault scenario, with the only distinguishing factor being the distance of the force from the shoulder along the leg (highlighted in the figure above). To address this, a rerun of the algorithm focuses only on classifying the differences between baseline, stuck wheel and stuck leg scenarios without excluding information about motor speed and direction from the training samples. Figure 38 presents the resulting new confusion matrix. An improvement can be seen in the classification of fault scenarios, while the false positive rate remains relatively stable compared to the first run.

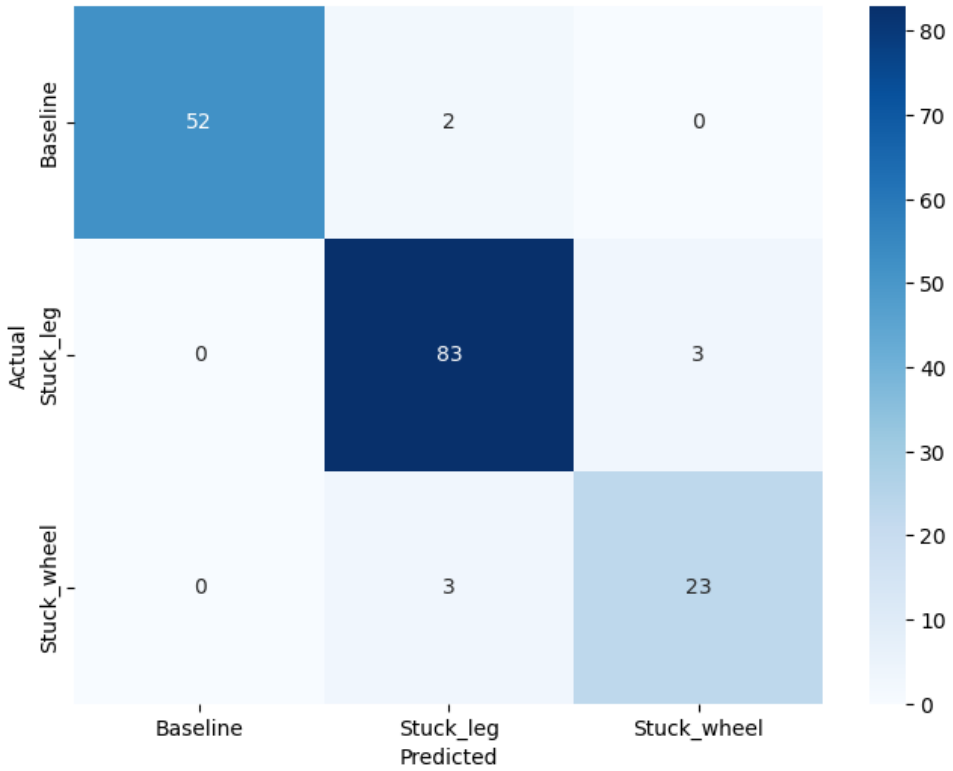


*Figure 38: Improved confusion matrix with two fault scenarios*

Table 5 shows the output of the algorithm after the second run. The four columns give a more thorough understanding of how well the model fits the data. Precision gives the percentage of correct positive predictions relative to total positive predictions (this includes true positives TP and false positives FP) as shown in ( III ).

$$Precision = \frac{TP}{TP + FP} \qquad (\text{III})$$

It shows the ability of the model to differentiate one scenario from all the others. It does not however give an idea of whether all samples corresponding to that class have been identified or not. In contrast to this there is the recall parameter. Recall, also known as the true positive rate, shows the percentage of correct positive predictions compared to the number of actual positives:

$$Recall = \frac{TP}{TP + FN} \qquad (\text{IV})$$

To merge information from both of these parameters, the F1-score is introduced. The F1-score is the harmonic mean of precision and recall and gives a more thorough understanding of the goodness of fit of the algorithm.

$$F1\text{-}score = 2 \cdot \frac{Precision \cdot Recall}{Precision + Recall} \qquad (\text{V})$$

Support, as the last column in the table, simply describes the number of samples for each class. Lastly, at the bottom of the table the accuracy of the algorithm is shown. It is the number of correct predictions compared to all predictions made in this run.

The overall accuracy of the algorithm improves from 86% in the initial training to 95% in the second run (compare accuracy in Table 5). This improvement can be attributed to the now additional information on the modes of the motors, which, as shown in section 6.2, have an impact on the measurements and the logistic regression parameters.

*Table 5: Classification report*

| | Precision | Recall | F1-score | Support |
|---|---|---|---|---|
| **Baseline** | 1.00 | 0.96 | 0.98 | 54 |
| **Stuck leg** | 0.94 | 0.97 | 0.95 | 86 |
| **Stuck wheel** | 0.88 | 0.88 | 0.88 | 26 |
| **Accuracy** | | | 0.95 | 166 |

The accuracy could be improved further by increasing the number of historic datasets used to train the classifier. Especially a higher number of stuck wheel data sets would enhance the classification, since for this class the support value is relatively low. Whether an improvement is necessary and warrants the extra resources this necessitates is dependent on the requirements defined for the FDI system. Since no particular requirements were specified, the demonstrated classifier, which shows a promising 95% accuracy, presents the best solution for the given problem of fault isolation within the scope of this thesis.

## 6.5 Weaknesses and Problems in the Investigation

This subchapter aims to discuss the weaknesses and problems encountered during the investigation, highlighting important factors that may have influenced the results and conclusions. The identified issues include the non-discrete design of the end stop, limitations in conducting stuck wheel tests, missing values for different rotation directions, and the omission of current changes due to an up- or downhill path. Understanding these weaknesses is crucial for interpreting the findings accurately and recognizing areas for further improvement in future studies.
Firstly, a significant weakness of the investigation is the design of the end stop.
With the used fail-safe version of an obstacle, compared to an unyielding version, a few major differences have to be considered. Firstly, the wrench does not pose an immovable obstacle, the torque limit inside the wrench is set by a counteracting spring force, which allows rotational movement before the internal mechanism jumps to the next position, when the force on the driving head exceeds the spring force. Furthermore, because of the spring and friction included in the reaction of the obstacle, the progression of the torque over the distance is not constant and not identical on every run. This lack of consistency and accuracy in the obtained values

can introduce uncertainty and potential errors in the torque measurements, consequently compromising the reliability and validity of the torque-related data. Thus, caution must be exercised when interpreting the findings.

Secondly, stuck wheel tests were conducted at the furthest point of the wheel from the shoulder, resulting in limited changes in the wheel motor current. The primary reason behind this limitation is that the torque triggers before the wheel motor current is significantly affected. This poses a challenge in differentiating between a stuck wheel and a stuck leg fault, especially when the leg is stuck close to the wheel. To address this issue, it is recommended to repeat the tests at different wheel positions, particularly those exerting a lower torque on the shoulder. By doing so, more discernible changes in the wheel motor current can be observed, before the shoulder torque sensor registers high loads, leading to better differentiation between a stuck wheel and a stuck leg.

Another limitation of the investigation is the absence of tests conducted for different rotation directions of the wheel and motor during stuck wheel testing. Due to constraints in the experimental setup, it was not possible to carry out these tests. This omission may restrict the generalizability of the findings. To enhance the comprehensiveness of the dataset and facilitate a thorough analysis of the system's performance under varying conditions, future studies should consider including stuck wheel tests for different rotation directions of both motors.

Lastly, the experiments in this study did not account for current and torque changes that may occur when traversing uphill and downhill paths. These maneuvers can exert additional strain on the system, leading to variations in torque and current values, and ultimately affecting the overall performance.

# 7 Conclusion

In conclusion, this scientific work focused on developing a method to detect and isolate stuck faults in the MMX leg module. Through comprehensive data analysis and statistical techniques, correlations, dependencies, and influences within the sensor measurements were investigated under various operating conditions.

The analysis first focused on data statistics, revealing the distribution of tests conducted for different scenarios and parameters. Exploring correlations and dependencies among sensor measurements provided insights into the behavior of motor currents and torque in relation to rotational speed and direction. The findings showed a linear relationship between motor current and commanded rotational speed, while the torque measurements exhibited a slight dependence on speed and a change in amplitude and sign with a change in rotation direction.

Furthermore, the study examined the influence of the two motors on each other, finding that the activation or operation of one motor did not significantly affect the current or torque measurements of the other motor. Moreover, the weight of the leg structure was found to have an impact on motor currents and torque, necessitating considerations for the influence of gravity during analysis and the adjustment of thresholds accordingly.

During the analysis, an interesting observation was made regarding the presence of torque oscillation during wheel movements, indicating an imbalance in the wheel and small torque peaks during gear meshing.

Regarding fault detection, the study explored different approaches to establish appropriate threshold values for identifying faults in the subsystem. An initially considered simplified model based on the current-speed relationship proved inadequate as it did not capture the torque, the primary indicator of faults. Instead, a signal-based approach was adopted, considering baseline tests and fault scenarios to determine threshold values that effectively detect faults without generating excessive false alarms.

To differentiate between fault scenarios, a machine learning algorithm was utilized, achieving a 95% accuracy in predicting specific fault scenarios with the given information on motor speed and direction. The algorithm demonstrated a low rate of false positives and no false negatives, highlighting its effectiveness in identifying normal leg behavior in the absence of faults.

In summary, this study offered valuable insights into fault detection and isolation in the MMX leg module. The analysis of correlations, dependencies, and influences within sensor measurements, coupled with the implementation of a machine learning algorithm, provides a framework for identifying and classifying faults, contributing to the reliability and performance of the Locomotion subsystem in the MMX Rover.

However, it is important to acknowledge the weaknesses and areas for improvement in future investigations. Limitations, such as the non-discrete design of the end stop, constraints in conducting stuck wheel tests, missing values for different rotation directions, and the omission of

current changes due to uneven paths highlight the need for further development. Future studies should aim to utilize an obstacle with more realistic characteristics, explore alternative stuck wheel testing positions, include stuck wheel tests for different rotation directions, and consider the impact of up- and downhill paths on the measurements to enhance the accuracy and comprehensiveness of the investigation.

# Bibliography


[1] K. Kuramoto *et al.*, 'Martian moons exploration MMX: sample return mission to Phobos elucidating formation processes of habitable planets', *Earth Planets Space*, vol. 74, no. 1, p. 12, Jan. 2022, doi: 10.1186/s40623-021-01545-7.

[2] 'Der Mars mit seinen Monden Deimos (oben) und Phobos'. https://www.dlr.de/de/aktuelles/nachrichten/2022/04/ein-rover-fuer-den-marsmond-phobos/der-mars-mit-seinen-monden-deimos-und-phobos.jpg (accessed Jun. 28, 2023).

[3] tekdeeps, 'The Idefix rover will roll over a Martian moon', *Tek Deeps*, Jun. 24, 2023. https://tekdeeps.com/the-idefix-rover-will-roll-over-a-martian-moon/ (accessed Jun. 28, 2023).

[4] 'Computersimulation des MMX-Rovers'. https://www.dlr.de/de/forschung-und-transfer/projekte-und-missionen/mmx/simulation-die-bedingungen-auf-phobos-realitaetsnah-nachbilden/computersimulation-des-mmx-rovers (accessed Jun. 28, 2023).

[5] https://www.jpl.nasa.gov, 'Mars Rover Spirit - Mars Missions - NASA Jet Propulsion Laboratory', *NASA Jet Propulsion Laboratory (JPL)*. https://www.jpl.nasa.gov/missions/mars-exploration-rover-spirit-mer-spirit (accessed Jun. 27, 2023).

[6] A. Wander and R. Förstner, 'Innovative Fault Detection, Isolation and Recovery Strategies On-Board Spacecraft: State of the Art and Research Challenges', Proc. of Deutscher Luft- und Raumfahrkongress, Berlin, 2012.

[7] R. Isermann, *Fault-Diagnosis Systems*. Berlin, Heidelberg: Springer, 2006. doi: 10.1007/3-540-30368-5.

[8] J. Gertler, 'Fault Detection and Diagnosis', in *Encyclopedia of Systems and Control*, J. Baillieul and T. Samad, Eds., Cham: Springer International Publishing, 1998, pp. 764–769. doi: 10.1007/978-3-030-44184-5_223.

[9] V. T. Do and U.-P. Chong, 'Signal Model-Based Fault Detection and Diagnosis for Induction Motors Using Features of Vibration Signal in Two-Dimension Domain', *Stroj. Vestn. – J. Mech. Eng.*, vol. 57, no. 09, pp. 655–666, Sep. 2011, doi: 10.5545/sv-jme.2010.162.

[10] X. Dai and Z. Gao, 'From Model, Signal to Knowledge: A Data-Driven Perspective of Fault Detection and Diagnosis', *IEEE Trans. Ind. Inform.*, vol. 9, no. 4, pp. 2226–2238, Nov. 2013, doi: 10.1109/TII.2013.2243743.

[11] J. Gertler, 'Fault Detection and Diagnosis', in *Encyclopedia of Systems and Control*, J. Baillieul and T. Samad, Eds., Cham: Springer International Publishing, 2021, pp. 764–769. doi: 10.1007/978-3-030-44184-5_223.

[12] J. Gertler, *Fault Detection and Diagnosis in Engineering Systems*. Boca Raton: CRC Press, 2019. doi: 10.1201/9780203756126.

[13] M. Azam, D. Pham, F. Tu, K. Pattipati, N. Patterson-Hine, and L. Wang, 'Fault detection and isolation in the NT-OMS/RCS', in *2004 IEEE Aerospace Conference Proceedings (IEEE Cat. No.04TH8720)*, Mar. 2004, pp. 2892-2902 Vol.5. doi: 10.1109/AERO.2004.1368096.

[14] J. M. Hilbe, *Logistic Regression Models*. London, UNITED KINGDOM: CRC Press LLC, 2009. Accessed: Jun. 20, 2023. [Online]. Available: http://ebookcentral.proquest.com/lib/dlr-ebooks/detail.action?docID=1633158

[15] H. van Elst, *An Introduction to Inductive Statistical Inference: from Parameter Estimation to Decision-Making (version 3)*. 2022. doi: 10.48550/arXiv.1808.10173.

[16] M. P. LaValley, 'Logistic regression', *Circulation*, vol. 117, no. 18, pp. 2395–2399, May 2008, doi: 10.1161/CIRCULATIONAHA.106.682658.

[17] R. Washington, 'On-board real-time state and fault identification for rovers', *Proc. 2000 ICRA Millenn. Conf. IEEE Int. Conf. Robot. Autom. Symp. Proc. Cat No00CH37065*, vol. 2, pp. 1175–1181, 2000, doi: 10.1109/ROBOT.2000.844758.

[18] R. Dearden, T. Willeke, R. Simmons, V. Verma, F. Hutter, and S. Thrun, 'Real-time fault detection and situational awareness for rovers: report on the Mars technology program task', in *2004 IEEE Aerospace Conference Proceedings (IEEE Cat. No.04TH8720)*, Mar. 2004, pp. 826-840 Vol.2. doi: 10.1109/AERO.2004.1367683.

[19] R. Venkataraman, P. Bauer, P. Seiler, and B. Vanek, 'Comparison of fault detection and isolation methods for a small unmanned aircraft', *Control Eng. Pract.*, vol. 84, pp. 365–376, Mar. 2019, doi: 10.1016/j.conengprac.2018.12.002.
[20] R. Dearden, D. Clancy, and D. Koga, 'Particle Filters for Real-Time Fault Detection in Planetary Rovers', Jan. 01, 2001. Accessed: May 10, 2023. [Online]. Available: https://ntrs.nasa.gov/citations/20020002861
[21] S. M. Zanoli, G. Astolfi, G. Bruzzone, M. Bibuli, and M. Caccia, 'Application of Fault Detection and Isolation Techniques on an Unmanned Surface Vehicle (USV)', *IFAC Proc. Vol.*, vol. 45, no. 27, pp. 287–292, 2012, doi: 10.3182/20120919-3-IT-2046.00049.
[22] S. R. K. Shilliday, E. W. McGookin, and D. G. Thomson, 'A Comparison of Forward and Inverse Simulation Methods for Fault Detection on a Rover', *2022 8th Int. Conf. Control Decis. Inf. Technol. CoDIT*, pp. 1432–1437, May 2022, doi: 10.1109/CoDIT55151.2022.9804106.
[23] F. Buse, A. Pignède, J. Bertrand, S. Goulet, and S. Lagabarre, 'MMX Rover Simulation - Robotic Simulations for Phobos Operations', in *2022 IEEE Aerospace Conference (AERO)*, Mar. 2022, pp. 1–14. doi: 10.1109/AERO53065.2022.9843391.
[24] S. Ulamec *et al.*, 'IAC-19-A3.4.B8 A ROVER FOR THE JAXA MMX MISSION TO PHOBOS', *Th Int. Astronaut. Congr.*.
[25] H.-J. Sedlmayr *et al.*, 'MMX - Development of a Rover Locomotion System for Phobos', in *2020 IEEE Aerospace Conference*, Mar. 2020, pp. 1–10. doi: 10.1109/AERO47225.2020.9172659.
[26] V. Langofer, R. Bayer, A. Kolb, and K. Sasaki, 'MMX Locomotion Subsystem: mechanics for extraterrestrial low gravity drive', Mar. 2023.
[27] J. Skibbe *et al.*, 'Fault Detection, Isolation and Recovery in the MMX Rover Locomotion Subsystem', Mar. 2023.
[28] '2020_Datenblatt-SensoInk-FR4-radial-H+K.pdf'. Accessed: Apr. 25, 2023. [Online]. Available: https://de.hoffmann-krippner.com/app/uploads/downloads/2020_Datenblatt-SensoInk-FR4-radial-H+K.pdf
[29] 'Infineon-TLE49X5L-DataSheet-v01_05-en.pdf'. https://www.infineon.com/dgdl/Infineon-TLE49X5L-DataSheet-v01_05-en.pdf?fileId=db3a304316f66ee80117549ac8b206b1 (accessed Apr. 25, 2023).
[30] R. Isermann, 'Model-based fault-detection and diagnosis – status and applications', *Annu. Rev. Control*, vol. 29, no. 1, pp. 71–85, Jan. 2005, doi: 10.1016/j.arcontrol.2004.12.002.
[31] 'Solar System Exploration: Planets: Mars: Moons: Phobos: Facts & Figures', Oct. 19, 2013. https://web.archive.org/web/20131019162634/http://solarsystem.nasa.gov/planets/profile.cfm?Object=Mar_Phobos&Display=Facts (accessed Jun. 19, 2023).

Hochschule München University of Applied Sciences

# Erklärung

**gemäß § 26 Abs. 7 ASPO**

Name: Merk

Vorname: Anna

Studiengang: LRB

Matrikel-Nr.: 01486219

Betreuer/in: Prof. Dr.-Ing. Daniel Ossmann

Hiermit erkläre ich, dass ich die Bachelorarbeit selbstständig verfasst, noch nicht anderweitig für Prüfungszwecke vorgelegt, keine anderen als die angegebenen Quellen oder Hilfsmittel benutzt, sowie wörtliche und sinngemäße Zitate als solche gekennzeichnet habe.

Gilching, 05.07.2023

Ort, Datum

Unterschrift